Materials Today Bio 32 (2025) 101759

Contents lists available at ScienceDirect

Materials Today Bio

journal homepage: www.journals.elsevier.com/materials-today-bio

A novel strategy for bone defect repair: Stromal cell-derived factor 1α sustained-release acellular fish scale scaffolds combined with injection of bone marrow mesenchymal stem cells promote bone regeneration

Shilong Su [a,b], Jinwu Bai [a,b], Ruideng Wang [a,b], Shan Gao [a,b], Rubing Zhou [c], Fang Zhou [a,b,*]

[a] Department of Orthopedics, Peking University Third Hospital, No.49 North Garden Road, Haidian, 100191, Beijing, China
[b] Engineering Research Center of Bone and Joint Precision Medicine, Peking University Third Hospital, No.49 North Garden Road, Haidian, 100191, Beijing, China
[c] Department of Orthopedics, Beijing Friendship Hospital, Capital Medical University, No.95 Yong'an Road, Xicheng, 100050, Beijing, China

ARTICLE INFO

Keywords:
Fish scale
SDF-1α
Cell injection
Tissue engineering
Bone regeneration

ABSTRACT

Patients with bone defects often have weak cell vitality and differentiation ability of endogenous bone marrow mesenchymal stem cells (BMSCs), which makes bone regeneration face challenges. At present, the bone tissue engineering strategies are mainly to build grafts by loading cells on scaffolds in vitro. These strategies face many difficulties that limit their clinical application. To this end, we developed a new strategy for bone defect repair, namely chemotactic cell-free scaffolds combined with BMSCs injection. We first prepared a polydopamine-functionalized acellular fish scale scaffold that can continuously release stromal cell-derived factor 1α (SDF-1α) (termed as SDF-1α/PAFS) in vivo for at least 10 days. The study results showed that the scaffold not only has excellent mechanical properties and good biocompatibility but also has reactive oxygen scavenging activity, immunomodulation, angiogenesis, and osteogenesis. More importantly, SDF-1α/PAFS can recruit postoperatively injected BMSCs into bone defects for bone repair. We constructed the mouse cranial bone defect model, and in vivo experimental results confirmed that the strategy of combining SDF-1α/PAFS with BMSCs injection can effectively promote bone defect repair. Overall, this study provides a promising strategy for bone defect repair, with better clinical convenience and operability.

1. Introduction

Bone regeneration and repair of bone defects caused by severe infection, trauma, and other reasons remains a major clinical challenge [1]. In recent years, bone tissue engineering has gradually become a promising treatment strategy. Although a variety of engineered scaffolds have been developed [2,3], natural acellular extracellular matrix materials have been widely studied for their multiple advantages, such as low immunogenicity, high biocompatibility, and good biodegradability [4,5]. Fish scales, as a biological waste in fisheries that have received little attention, are composed of an extracellular matrix, mainly hydroxyapatite and collagen, which is similar to the composition of bone tissue [6]. Compared with collagen derived from terrestrial organisms, collagen derived from marine organisms has been shown to have good biocompatibility and low immunogenicity [7]. Fish scales also have a "Bouligand" microstructure composed of layers of collagen fibers with different orientations, which provides excellent mechanical properties through the synergy of deformation mechanisms [8]. Studies have reported that acellular fish scales have a good ability to induce osteogenic differentiation [9–11]. Therefore, acellular fish scale scaffold (AFS) is a potential choice for bone tissue engineering scaffolds.

Ideal bone defect repair should be able to recruit a sufficient number of normally active bone marrow mesenchymal stem cells (BMSCs) and retain them in the bone defect. Endogenous BMSCs play a key role in successful bone defect repair [12]. However, bone defects often occur with comorbidities as pathological factors, such as infection, tumors, and osteoporosis, which can cause systemic or local microenvironment disorders, resulting in impairment of the functions of endogenous BMSCs, including reduced vitality, poor migration ability, and reduced osteogenic differentiation activity [12–15]. These factors limit their role

* Corresponding author. Department of Orthopedics, Peking University Third Hospital, No.49 North Garden Road, Haidian, 100191, Beijing, China.
E-mail addresses: sushilong2020@163.com (S. Su), med_bai.jinwu@stu.pku.edu.cn (J. Bai), wangruideng0467@bjmu.edu.cn (R. Wang), gaoshan@bjmu.edu.cn (S. Gao), rubingzhou@pku.edu.cn (R. Zhou), zhouf@bjmu.edu.cn (F. Zhou).

https://doi.org/10.1016/j.mtbio.2025.101759
Received 25 February 2025; Received in revised form 2 April 2025; Accepted 9 April 2025
Available online 10 April 2025

in bone defect repair. To solve this problem, traditional tissue engineering is to load BMSCs on scaffolds in vitro and then implant them in vivo. However, this mode is very inconvenient when cultured in vitro, and there is also concern that the loaded cells will be inactivated before implantation [16]. Moreover, after implantation in vivo, most of the loaded cells are rapidly inactivated in the damaged microenvironment, and only a few cells ultimately participate in the formation of target tissues [12,16,17]. To solve these problems, developing a chemotactic cell-free scaffold that can recruit postoperatively injected BMSCs to bone defect sites in vivo may be a promising method.

Stromal cell-derived factor 1α (SDF-1α) can regulate stem cell homing [18] and migration [19] through C-X-C chemokine receptor type 4 (CXCR4) [20]. CXCR4 is constitutively expressed on the surface of most stem/progenitor cells, including endothelial progenitor cells [21] and osteogenic progenitor cells [22], with BMSCs expressing both SDF-1α and CXCR4 [23]. Therefore, at the cellular level, SDF-1α induces the migration of BMSCs through its receptor, which has been reported in multiple studies [24–26]. SDF-1α has also been shown to improve angiogenesis [21,27]. But what we need to note is that SDF-1α not only recruits endogenous stem cells but also excessive inflammatory cells [28,29]. The microenvironment of the bone defect site itself is in a state of high levels of reactive oxygen species (ROS) and inflammatory disorders that manifest as long-term pro-inflammatory responses [30–32], which will inevitably aggravate the deterioration of the microenvironment. In addition, the current common method for introducing SDF-1α into scaffolds is direct protein incorporation [29,33,34]. When SDF-1α is bound to the scaffold in this way, it diffuses and degrades too quickly, and shows only a short-term effect on cell recruitment. To solve the above problems, functionalizing the scaffold with polydopamine (PDA) is a good solution. By simply immersing the scaffold in an aqueous dopamine solution, PDA can easily form a 50-nm-thick coating on the surface of the scaffold [35]. The PDA coating has a special viscosity and adsorption effect, which can fix cytokines on the surface of the scaffold without affecting the activity and release them slowly [36,37]. More importantly, PDA also has efficient redox ability, which can reduce ROS levels [38,39]. At the same time, it also has immunomodulatory activity, which can reduce the polarization of M1 macrophages and activate the polarization of M2 macrophages, exerting an anti-inflammatory effect

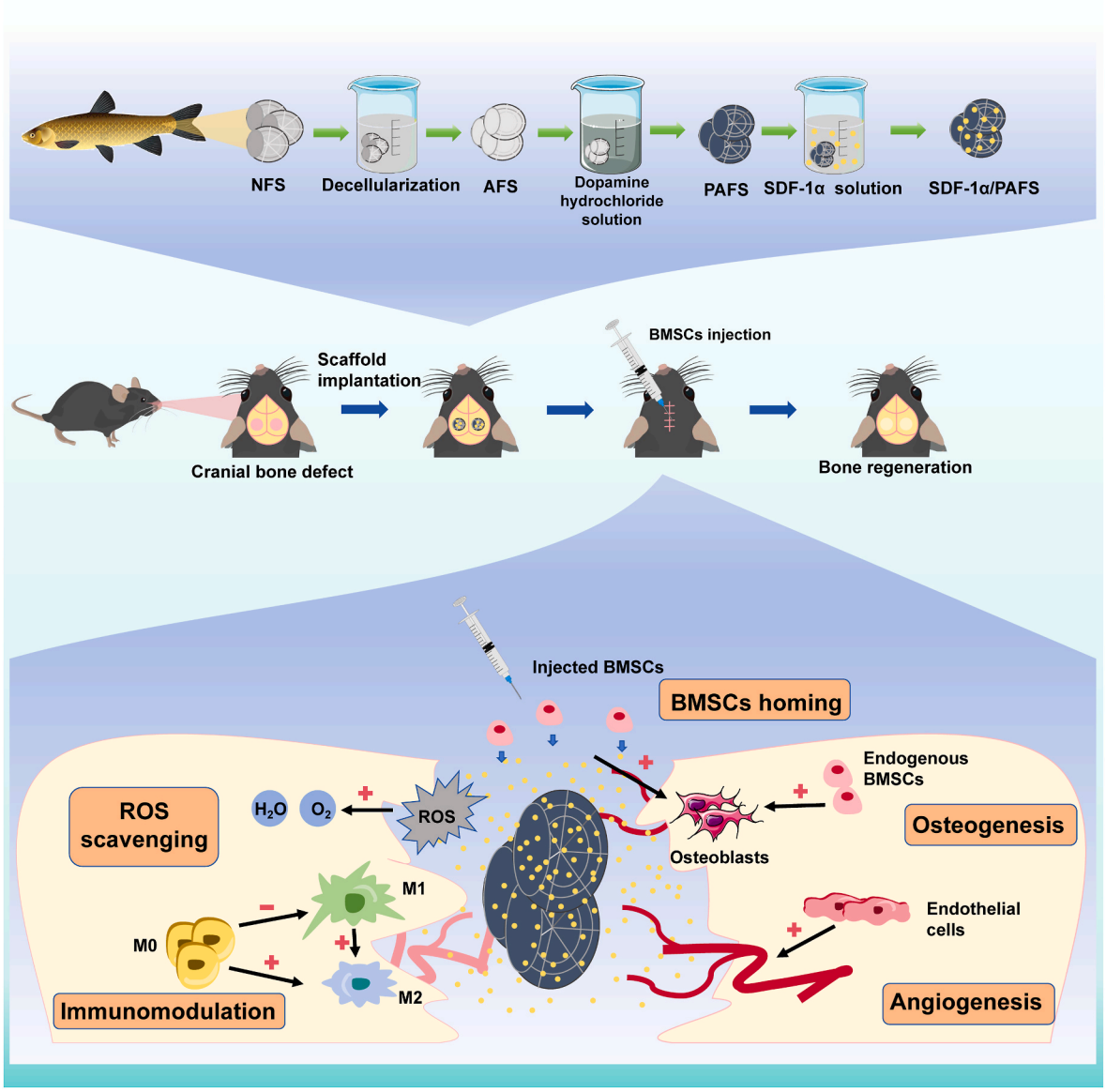

Fig. 1. Schematic illustration of a novel strategy for the treatment of bone defects of combining postoperative injection of BMSCs and the polydopamine-functionalized acellular fish scale scaffold with sustained release of SDF-1α, which can recruit exogenous BMSCs, and also has ROS scavenging activity, immunomodulation, angiogenesis, and osteogenesis.

[40,41]. Therefore, after the scaffold is functionalized with PDA (PAFS), it can not only have the ability to slowly release SDF-1α, but also regulate the damaged microenvironment of the bone defect site.

In summary, we developed a polydopamine-functionalized acellular fish scale scaffold with sustained release of SDF-1α (SDF-1α/PAFS), which can recruit BMSCs injected postoperatively to bone defects for bone repair in vivo. The scaffold can release SDF-1α slowly, recruit exogenous BMSCs, and also has ROS scavenging activity, immunomodulation, angiogenesis, and osteogenesis, which can be used to repair bone defects (Fig. 1). In this study, we evaluated the scaffold's application potential in bone regeneration from multiple aspects including scaffold characteristics, SDF-1α binding and sustained release ability, cell compatibility and cell migration, ROS scavenging activity, immunomodulation, and angiogenesis and osteogenic differentiation ability in vitro and in vivo. This multifunctional scaffold and repair strategy not only has multiple biological activities but also has excellent mechanical properties and low-cost accessibility. More importantly, it avoids the complex process and rigorous care of in vitro cell loading of traditional bone tissue grafts, with better clinical convenience.

2. Experimental section

2.1. Materials

Fish scales were isolated from Grass carps. Tris-hydrochloride (Tris-HCl), Triton X-100, ethylenediamine tetraacetic acid (EDTA), and ribonuclease A were purchased from Bioroyee (Beijing, China). Deoxyribonuclease I was procured from Mreda (Beijing, China). Dopamine hydrochloride was purchased from Sigma-Aldrich (Carlsbad, USA). SDF-1α was purchased from PeproTech (Rocky Hill, USA). Fetal bovine serum (FBS), α-MEM, penicillin-treptomycin, and trypsin were purchased from Gibco (Grand Island, USA). Dexamethasone, ascorbic acid, β-Sodium Glycerol 3-phosphate, bovine serum albumin (BSA), and phosphate buffered saline (PBS) were purchased from Solarbio (Beijing, China). Endothelial cell medium was purchased from ScienCell (Carlsbad, USA).

2.2. Fabrication of SDF-1α/PAFS

2.2.1. Preparation of PAFS

The native fish scales (NFS) were obtained from grass carp, and then the soft tissues on the surface of NFS were removed. The fish scales were immersed in 10 mM Tris-HC1 buffer containing 0.1 % EDTA (4 °C, 24 h), and the cell components of the fish scales were then removed with 1 % Triton X-100 for 4 days. Next, the fish scales were digested with nuclease solution (containing 500U/mL of deoxyribonuclease I and 1 mg/mL of ribonuclease A) at 37 °C for 24 h. After cleaning, AFS was obtained [42]. Afterwards, under mechanical stirring, AFS was immersed in dopamine hydrochloride solution (2 mg/ml, pH 8.5) at room temperature for 24 h for PDA functionalization. Finally, PAFS was sterilized with 75 % ethanol and ultraviolet light, freeze-dried, and stored for later use.

2.2.2. SDF-1α binding assay in vitro

To determine the SDF-1α binding ability of PAFS, 100 μL of the same concentration of SDF-1α solution was incubated with AFS or PAFS (about 5 mm × 5 mm, n = 3) at 4 °C for 24 h under different concentration gradients (0, 0.5, 1.0, 1.5, 2.0 and 2.5 μg/mL). We collected solutions containing unbound SDF-1α and used the SDF-1α enzyme-linked immunosorbent assay (ELISA) kit (Multisciences, China) for quantitative analysis. Finally, we selected a 2.5 μg/mL concentration of SDF-1α solution to prepare SDF-1α/PAFS.

2.3. Evaluation of scaffolds

2.3.1. Decellularization evaluation

We evaluated the decellularization effect and the effect of the decellularization process on extracellular matrix content. NFS and AFS were first decalcified, paraffin-embedded, and then stained with Hematoxylin and eosin (H&E) and 4',6-diamidino-2-phenylindole (DAPI) (n = 3). The total DNA of NFS and AFS was extracted using a marine animal tissue genomic DNA extraction kit (Bioroyee, China) and then determined by a spectrophotometer (DHS, China) (n = 5). In addition, we also used Fourier transform infrared spectroscopy (FTIR) to detect sections of NFS and AFS and obtain their infrared spectra (n = 3) [43,44]. By integrating the peak areas of the amide I peak (1720-1590 cm^{-1}) and phosphate peak (1200-900 cm^{-1}) respectively, the content of collagen and hydroxyapatite in the scaffolds was semi-quantitatively described [44–46].

2.3.2. Characterization of scaffolds

We used scanning electron microscopy (SEM) to observe the surface morphology of AFS and SDF-1α/PAFS, and energy-dispersive X-ray spectroscopy (EDS) (JSM-7900F, JEOL, Japan) to detect the elemental distribution of carbon (C), calcium (Ca) and phosphorus (P) in the scaffolds (n = 3). The in vitro swelling and degradation behavior of the scaffolds were also tested: the freeze-dried scaffolds (weight: M_0) were immersed in PBS solution (n = 3), soaked at 37 °C for 48 h to fully swell, and the wet weight of each scaffold (M_1) was measured. Then they were immersed in fresh PBS again, and the remaining weight of the scaffolds (M_X) was recorded at the planned time points (2, 4, 6, and 8 weeks). The formulas are as follows: swelling rate = $(M_1\text{-}M_0)/M_0 \times 100$ % and degradation rate = $(M_1\text{-}M_X)/M_1 \times 100$ %. To evaluate the mechanical properties of the scaffolds, the scaffolds were tested using the atomic force microscope (AFM) (Bruker, Germany) to obtain force-displacement curves (n = 3), and then Nanoscope Analysis software (Version 3.0, Bruker, Germany) was used to calculate the Young's modulus of the scaffolds. Moreover, we evaluated the controlled release of SDF-1α from the scaffolds. Briefly, add 100 μL solution containing 250 ng SDF-1α to dried AFS and PAFS, respectively, and incubate at 4 °C for 24 h (n = 3). SDF-1α/AFS and SDF-1α/PAFS were then soaked in 100 μL PBS and incubated on a shaker platform (37 °C, 100 rpm). During 7 days, PBS was collected every 24 h and replaced with an equal amount of fresh PBS. The SDF-1α content in the collected PBS was measured using the SDF-1α ELISA kit (Multisciences, China), and the cumulative release amount was calculated.

2.4. In vitro experiments

2.4.1. Biocompatibility assay

BMSCs (2×10^4 cells, Passage 4) were seeded onto the scaffolds (n = 3). After 1 and 3 days of culture, the cells were stained using a live/dead cell kit (Servicebio, China), and the cell viability was calculated. We used fluorescence microscopy and SEM to observe the adhesion and morphology of cells on the scaffolds. Specifically, the cytoskeleton and nucleus were stained with FITC-phalloidin and DAPI (Solarbio, China), respectively, and then observed with a fluorescence microscope (Nikon, Japan). The scaffolds with cells were fixed with 2.5 % glutaraldehyde, dried, and observed using SEM (JSM-7900F, JEOL, Japan). In addition, cell proliferation was quantified using a Cell Counting Kit-8 (CCK-8) (Fude Biological, China) after 1, 3, 5, and 7 days of culture.

2.4.2. Chemotaxis assay

The AFS and SDF-1α/PAFS were soaked in 200 μL PBS and incubated on a shaker platform (37 °C, 100 rpm) for 3 days, with PBS replaced every 24 h. Then, AFS and SDF-1α/PAFS were transferred to the lower chambers of the 24-well Transwell plate (Corning, USA) and 600 μL of the serum-free medium was added, with no scaffold added as the control group (n = 3). BMSCs (2×10^4 cells, Passage 4) were added to the upper chambers (8-μm pore) and 100 μL serum-free medium was added. After incubation for 24 h, cells were fixed in 4 % paraformaldehyde. The cells on the upper surface of the upper chamber were wiped off with a cotton swab, the migrated cells were stained with crystal violet solution, and

finally observed and counted under an optical microscope.

In addition, we also conducted a scratch assay. The scaffolds were transferred to the upper chambers of the 24-well Transwell plate and BMSCs (1×10^5 cells, Passage 4) were seeded in the lower chambers (n = 3). After 24 h of incubation, the scratches were completed with a 200-μL pipette tip and suspended cells were washed out with PBS. The medium was then replaced with the serum-free medium. After 0 and 24 h, scratches were photographed with an optical microscope, and cell migration rate was calculated.

2.4.3. ROS scavenging activity

The ROS scavenging activity of the scaffolds was evaluated by 1,1-diphenyl-2-picrylhydrazyl (DPPH) scavenging efficiency, the cellular protective effect under oxidative stress, and intracellular ROS scavenging ability. The DPPH scavenging efficiency was determined using the DPPH scavenging efficiency assay kit (Yuanye, China) according to the instructions, with vitamin C (40 μg/ml) as a positive control (n = 3). BMSCs (2×10^4 cells, Passage 4) were seeded in a 48-well plate, and after 24 h of culture, the scaffolds were added, and the medium was replaced with the medium containing 200 μM H_2O_2 (n = 3). After another 24 h of culture, the scaffolds and medium were removed, and the cellular protective effect under oxidative stress was evaluated using a live/dead cell kit (Servicebio, China) and CCK-8 (Fude Biological, China), respectively. In addition, when the culture continued for 2 h, ROS production in BMSCs was detected using a reactive oxygen species detection kit (2′,7′-dichloro fluorescein diacetate, DCFH-DA, Beyotime, China) (n = 3), and quantitative analysis was performed using a multifunctional microplate reader (Molecular Devices, USA).

2.4.4. ELISA

RAW264.7 cells (1×10^4 cells) were seeded on the scaffolds (n = 5). After 3 days of culture, the cell supernatant from each group was collected, and then the contents of tumor necrosis factor-α (TNF-α) and interleukin-10 (IL-10) were determined according to the instructions of the ELISA kits (Multisciences, China).

2.4.5. Alkaline phosphatase (ALP) activity and alizarin red staining (ARS)

BMSCs (1×10^4 cells, Passage 3) were seeded on the scaffolds and the osteogenic induction medium was added (n = 3). After 7 and 14 days of culture, the cells were fixed and then stained with an ALP staining kit (Beyotime, China). In addition, the ALP activity of cells was measured using an ALP activity assay kit (Beyotime, China) and normalized based on the total protein content measured by the BCA protein assay kit (Beyotime, China). ARS staining was also performed using an ARS staining kit (Beyotime, China) at 21 days of culture. To quantify the calcium content, calcium nodules were dissolved in 10 % cetylpyridinium chloride solution and the absorbance was measured at 570 nm.

2.4.6. Immunofluorescent (IF) staining

After 3 days of co-culture of RAW264.7 cells or human umbilical vein endothelial cells (HUVECs) with scaffolds and 14 days of osteogenic induction of BMSCs with scaffolds (n = 3), the expression of relevant marker proteins was observed by IF staining. Briefly, cells were fixed, permeabilized, blocked, and incubated with specific primary antibodies overnight. The relevant primary antibodies are as follows: CD86 (1:200, 13395-1-AP, Proteintech), CD206 (1:200, 18704-1-AP, Proteintech), CD31 (1:200, 11265-1-AP, Proteintech), RUNX2 (1:100, 20700-1-AP, Proteintech), OPN (1:200, 22952-1-AP, Proteintech) and COL1 (1:100, 14695-1-AP, Proteintech). The next day, cells were incubated with fluorescent secondary antibodies, cell nuclei were stained with DAPI (Solarbio, China), and images were then acquired with a fluorescent microscope (Nikon, Japan).

2.4.7. Transwell assay

The scaffolds were placed in the lower chambers of a 24-well Transwell plate with 600 μL of medium, and then 2×10^4 HUVECs resuspended in 100 μL of serum-free medium were added to the upper chambers (n = 3). After 24 h of culture, the cells were fixed and the cells on the upper surface of the upper chambers were wiped off with a cotton swab. The migrated cells were stained with crystal violet solution and finally observed and counted under an optical microscope.

2.4.8. Tube formation assay

The scaffolds were placed in the upper chambers of a 24-well Transwell plate, and then HUVECs (8×10^4 cells) were seeded in the Matrigel-coated lower chambers (BD Bioscience, USA) (n = 3). After 8 h of incubation, images of each well were taken using an optical microscope, and tube formation was assessed using ImageJ software.

2.4.9. Quantitative real-time PCR (qRT-PCR)

After RAW264.7 cells and HUVECs were co-cultured with scaffolds for 3 days and 7 days, respectively, and BMSCs were induced with the scaffolds for 14 days (n = 3), the total RNA of the cells was extracted using SteadyPure Universal RNA Extraction kit (Accurate Biotechnology, China), and cDNA was synthesized by reverse transcription using Premix RT Evo M-MLV kit (Accurate Biotechnology, China). Finally, qRT-PCR was performed using the SYBR Green Premix Pro Taq HS kit (Accurate Biotechnology, China). mRNA expression levels were normalized using GAPDH and relative quantification was performed using the $2^{-\Delta\Delta Ct}$ method. Primer sequences included GAPDH, CD86, CD206, TNF-α, VEGFA, HIF1A, RUNX2, OPN and COL1A1, and were listed in Table S1.

2.4.10. RNA sequencing

After 14 days of osteogenic induction of BMSCs with SDF-1α/PAFS, we performed transcriptome analysis to explore the potential mechanism (n = 3). Briefly, the total RNA of cells was extracted with Trizol reagent, and then the samples were sent to Shanghai Majorbio Biotechnology Co., Ltd. for sequencing. DESeq2 was used for differential expression analysis. Kyoto Encyclopedia of Genes and Genomes (KEGG) pathway enrichment analysis was also performed. All analyses were performed using Majorbio's cloud platform.

2.5. In vivo experiments

2.5.1. Animal model

Eight-week-old C57BL/6J mice were used to establish cranial bone defect models. The study protocol was approved by the Animal Care and Use Committee of Peking University Health Science Center (DLASBD0205). After anesthesia, round full-thickness bone defects with a diameter of 3 mm were made on both sides of the parietal bone using a trephine. AFS and SDF-1α/PAFS were implanted into the bone defects, respectively, and the dura mater was protected from damage during the operation. No scaffold was placed in the control group. In the SDF-1α/PAFS + BMSCs group, 10^6 BMSCs in 20 μL PBS were injected into the vicinity of the bone defects at the center of the top of the mouse's skull 4 days postoperatively. For the control, AFS, and SDF-1α/PAFS groups, the same volume of PBS was injected.

2.5.2. SDF-1α release assay in vivo

The mice in the control and SDF-1α/PAFS + BMSCs groups were sacrificed on day 1, day 3, day 5, day 7, and day 9 after surgery respectively for cardiac blood collection (n = 3). The concentration of SDF-1α in serum was detected using the SDF-1α ELISA kit (Multisciences, China).

2.5.3. BMSCs labeling and tracking

To track the migration of injected BMSCs, BMSCs were pre-stained with DiR stain. In addition to injecting DiR-labeled BMSCs into the SDF-1α/PAFS + BMSCs group, mice in the AFS group were also injected with DiR-labeled BMSCs for control (n = 3). A small animal in vivo imaging system (IVIS Spectrum, PerkinElmer, USA) was used to image

the fluorescence intensity and distribution in the heads of mice on the day of cell injection and on days 8 and 12 after surgery. Finally, the mice were sacrificed, the skulls were obtained, and this system was used to image again.

2.5.4. Micro-CT evaluation

The mice were sacrificed 4 and 8 weeks after surgery, and skulls were obtained and fixed with 4 % paraformaldehyde (n = 3). The entire skull was then scanned using micro-CT (Siemens, Germany), and three-dimensional reconstruction was performed using software, while the bone volume as a percentage of tissue volume (BV/TV), and the trabecular number (Tb.N), thickness (Tb.Th), and separation (Tb.Sp) were calculated.

2.5.5. Histological evaluation

After micro-CT evaluation, the skulls were decalcified, dehydrated, embedded in paraffin, and then made into 5 μm sections. The sections were stained with H&E and Masson's trichrome to assess bone regeneration. Subsequently, in vivo immunomodulation, osteogenesis, and angiogenesis were further evaluated by immunohistochemical staining of immunomodulation-related proteins (CD86 and CD206), osteogenesis-related proteins (RUNX2 and OCN) and angiogenesis-related proteins (CD31 and EMCN). In addition, we also obtained the hearts, livers, spleens, lungs, and kidneys of mice and stained them with H&E to evaluate the biological safety of the scaffolds in vivo.

2.6. Statistical analysis

The quantitative results were presented as mean ± standard deviation. The student's t-test was used for comparisons between two groups, and one-way analysis of variance (ANOVA) and Tukey's post-hoc test were used for comparisons between multiple groups. Statistical analysis was performed using GraphPad Prism software (version 10.0), and the differences were considered statistically significant when $p < 0.05$.

3. Results

3.1. Preparation and decellularization evaluation of scaffolds

The native fish scales (NFS) were harvested from grass carp. After decellularization and PDA functionalization, we first evaluated the binding ability of PAFS to SDF-1α. We found that as the concentration of SDF-1α solution increased, the binding amount of PAFS also increased linearly, and at different concentrations, the binding amount of PAFS was all higher than that of AFS. This showed that PAFS had good binding ability to SDF-1α (Fig. 2A). Finally, we selected a 2.5 μg/mL concentration of SDF-1α solution to prepare SDF-1α/PAFS. In addition, after decellularization, the fish skin on the surface of AFS was completely removed and the scales became more transparent. Histological staining showed that no cell nuclei were seen in AFS (Fig. 2B). DNA content determination results showed that the DNA content in AFS was significantly reduced and below 50 ng/mg, which is the criterion for successful decellularization (Fig. 2C) [47]. Fourier transform infrared spectroscopy (FTIR) results confirmed that fish scales are mainly composed of collagen and hydroxyapatite (Fig. S1A). Further analysis results showed that the collagen and hydroxyapatite contents in AFS were reduced by approximately 26.22 % and 26.28 % (Fig. 2D), respectively, compared with NFS.

3.2. Characterization of scaffolds

SDF-1α/PAFS was dark brown (Fig. 2E). The surface structure of the scaffolds was observed by scanning electron microscopy (SEM), and it was found that the surface of AFS was a regular three-dimensional topological structure with directional ridges and grooves. The surface structure of SDF-1α/PAFS was similar to that of AFS, but its ridges and grooves were smoother (Fig. 2E). Energy-dispersive X-ray spectroscopy (EDS) analysis of the element distribution on the surface of the scaffolds showed that the C, Ca, and P elements were evenly distributed on the surface of both scaffolds. Among them, the surface content of the above elements of SDF-1α/PAFS was lower due to the surface functionalization of PDA (Fig. 2E). The swelling rate and degradation rate of the scaffolds were also evaluated. The swelling rates of the two kinds of scaffolds were similar and both were above 60 % (Fig. S1B). We measured the degradation rate of the scaffolds at 2, 4, 6, and 8 weeks, and found that the degradation rates of the two kinds of scaffolds were similar in the first 6 weeks, but the degradation rate of AFS was higher in the 8th week (Fig. 2F). This may be because the surface functionalization of PDA delayed the degradation of SDF-1α/PAFS. The results of mechanical properties analysis showed that Young's moduli of the scaffolds were similar, 5.90 ± 1.17 GPa (AFS) and 6.01 ± 1.90 GPa (SDF-1α/PAFS), respectively (Fig. 2G). Taking advantage of the special adsorption effect of PDA, SDF-1α/PAFS can be used as a local delivery system for the sustained release of SDF-1α. Our in vitro experimental results showed that the release rate of SDF-1α from SDF-1α/PAFS was significantly slower than that from SDF-1α/AFS. After 7 days of liquid immersion, the cumulative release of SDF-1α/AFS was about 94.00 ± 3.79 %, while that of SDF-1α/PAFS was only about 33.08 ± 0.89 % (Fig. 2H).

3.3. Biocompatibility of scaffolds

We directly seeded BMSCs on the scaffolds to explore the biocompatibility of the scaffolds. After 1 and 3 days of co-culture, live/dead staining showed that most of the cells on the scaffolds were stained fluorescent green (living cells), and very few were stained red (dead cells) (Fig. 3A). Quantitative analysis showed that the cell viability on the scaffolds was not significantly different from that in the control group (Fig. S2A). The results of CCK-8 also confirmed that the cells on the two kinds of scaffolds proliferated well (Fig. S2B). We observed the adhesion morphology of BMSCs on the scaffolds. We first used a fluorescence microscope to observe and found that the cells on the scaffolds were arranged and grew along the ridges and grooves on the surface of the scaffolds. Among them, the cells on SDF-1α/PAFS were arranged more regularly and adhered more tightly. After 3 days of co-culture, the number of cells on the scaffolds increased as the cells continued to proliferate. The cells on AFS gradually arranged in disorder, while the cells on SDF-1α/PAFS showed a more obvious regular distribution and remained tightly adhered (Fig. 3B). Next, we used SEM for further observation and found similar results. The cells on SDF-1α/PAFS had more pseudopods, were more significantly distributed along the ridges and grooves, and adhered more tightly (Fig. 3C).

3.4. Chemotaxis of scaffolds

To verify whether SDF-1α/PAFS can induce directional migration of BMSCs, we performed a Transwell assay and a scratch assay. In addition, to better simulate the recruitment of BMSCs in vivo, the scaffolds were first immersed in PBS for 3 days. The final results confirmed that the number of migrated BMSCs and cell migration rate in the SDF-1α/PAFS group were both significantly higher than those in the AFS group and the control group, while there was no significant difference between the AFS group and the control group (Fig. 3D).

3.5. ROS scavenging activity of scaffolds

We evaluated the ROS scavenging activity of the scaffolds from multiple aspects. First, we evaluated the DPPH scavenging efficiency of the scaffolds and found that the DPPH scavenging efficiency of SDF-1α/PAFS was significantly higher than that of AFS, reaching a level comparable to that of the antioxidant vitamin C (Fig. 4A). Next, we used H_2O_2 to induce oxidative stress and evaluated the protective effect of the scaffolds on BMSCs. The results showed that under oxidative stress, a

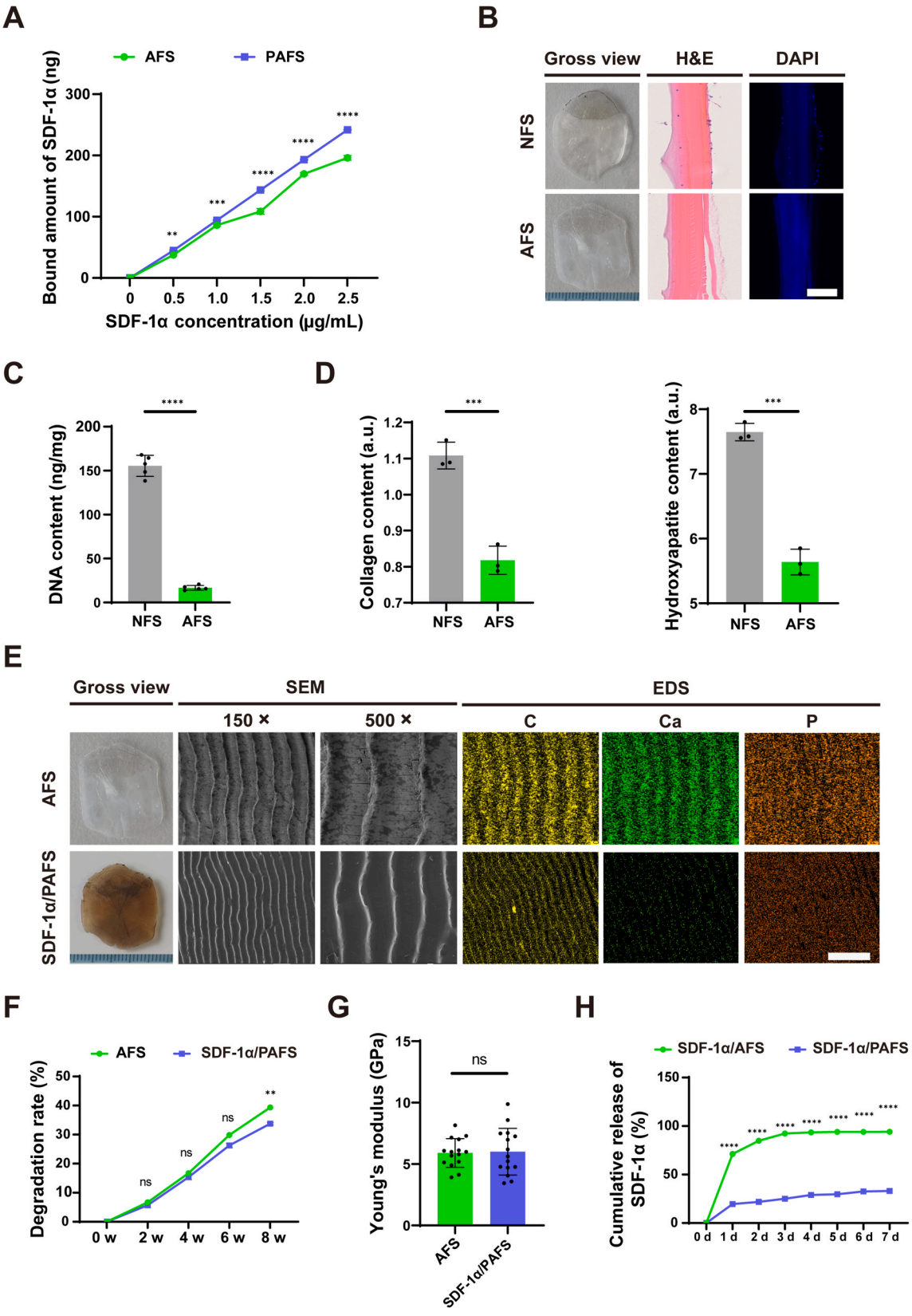

Fig. 2. Decellularization evaluation and characterization of scaffolds. **A.** The SDF-1α binding curves of AFS or PAFS. **B.** Gross view and histological staining of NFS and AFS. Scale bar = 100 μm. **C.** Quantitative analysis of DNA content of NFS and AFS. **D.** Semi-quantitative analysis of collagen and hydroxyapatite contents of NFS and AFS. **E.** Gross view, SEM, and EDS elemental mapping images of AFS and SDF-1α/PAFS. Scale bar = 250 μm. Quantitative analysis of the degradation rate (**F**) and Young's modulus (**G**) of AFS and SDF-1α/PAFS. **H.** The cumulative release curves of SDF-1α of SDF-1α/AFS or SDF-1α/PAFS in-vitro. The results were presented as mean ± SD (ns: no significant differences, *: $p < 0.05$, **: $p < 0.01$, ***: $p < 0.001$, ****: $p < 0.0001$).

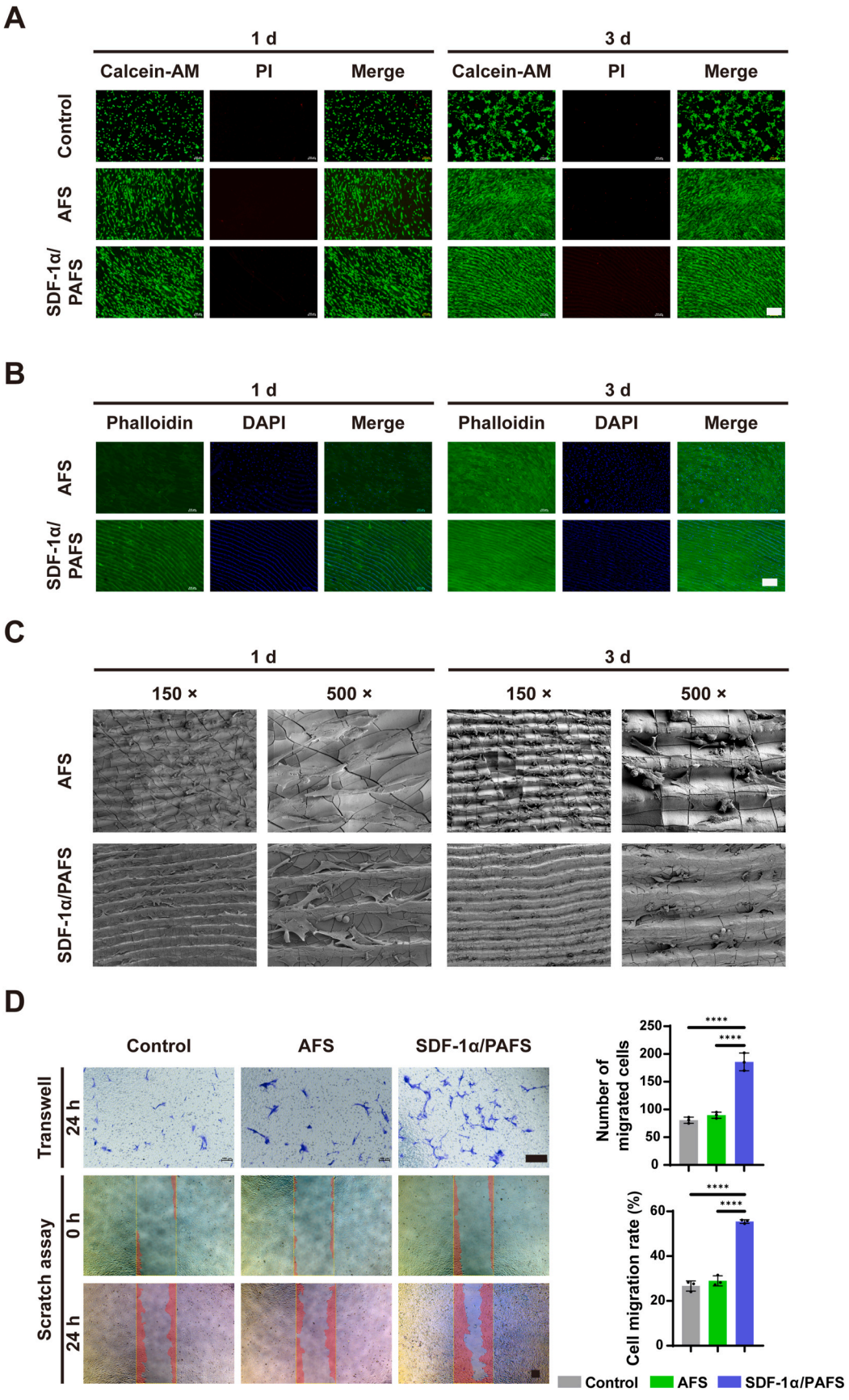

(caption on next page)

Fig. 3. Biocompatibility and chemotaxis of scaffolds. **A.** Live/dead staining of BMSCs cultured on the scaffolds on days 1 and 3. Scale bar = 200 μm. **B.** Fluorescence microscopy images of the phalloidin/DAPI staining of BMSCs cultured on the scaffolds on days 1 and 3. Scale bar = 200 μm. **C.** The representative SEM images of BMSCs cultured on the scaffolds on days 1 and 3. **D.** Comparison of the chemotaxis of AFS and SDF-1α/PAFS after rinsed 3-day on the migration of BMSCs through the Transwell assay and scratch assay. Scale bar = 200 μm. The results were presented as mean ± SD (ns: no significant differences, *: $p < 0.05$, **: $p < 0.01$, ***: $p < 0.001$, ****: $p < 0.0001$).

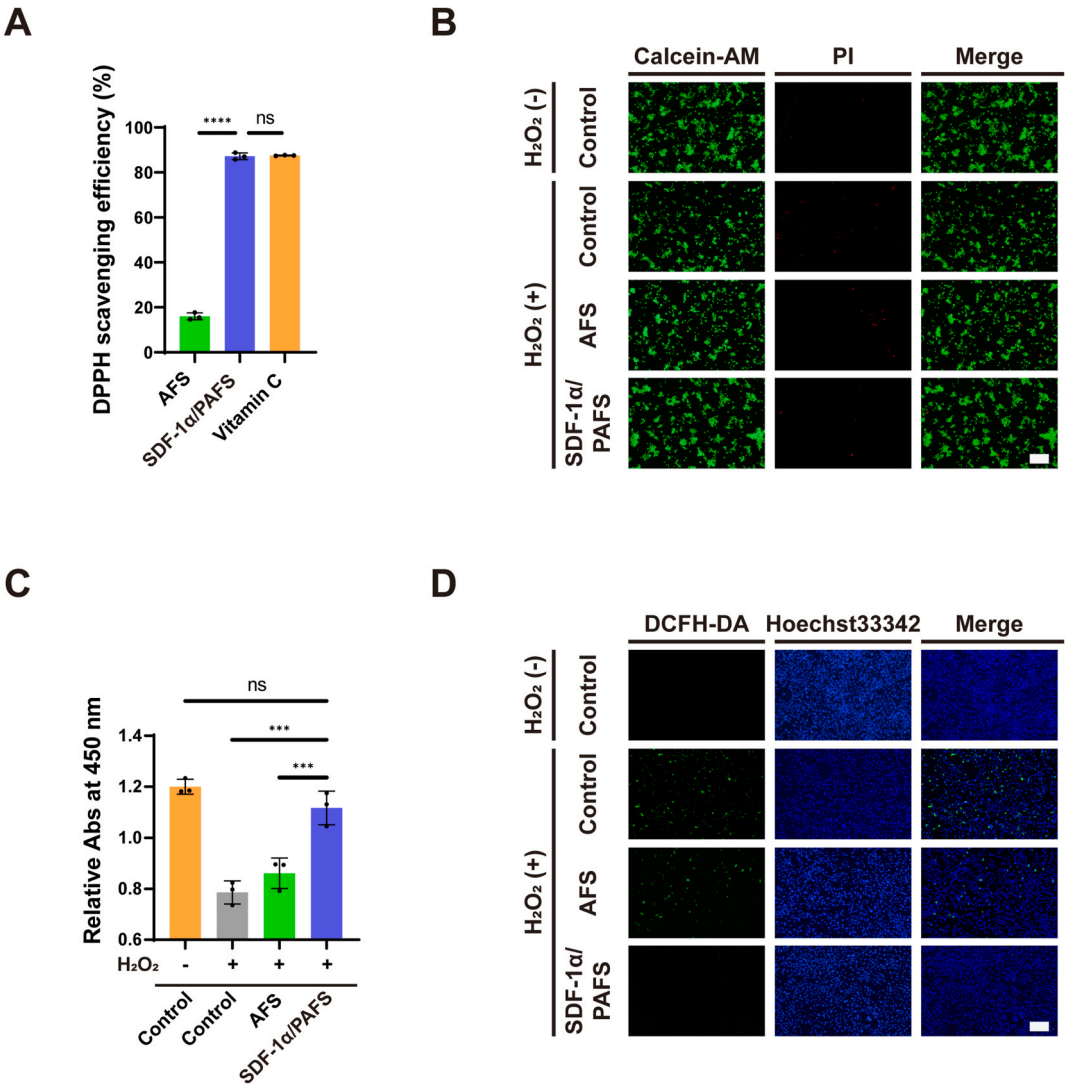

Fig. 4. ROS scavenging activity of scaffolds. **A.** DPPH scavenging efficiency of scaffolds. Live/dead staining images (**B**) and CCK-8 assay results (**C**) of BMSCs after co-culture with scaffolds and H_2O_2 for 24 h. Scale bar = 200 μm. **D.** Intracellular ROS fluorescent images of BMSCs after co-culture with scaffolds and H_2O_2 for 2 h. Scale bar = 200 μm. The results were presented as mean ± SD (ns: no significant differences, *: $p < 0.05$, **: $p < 0.01$, ***: $p < 0.001$, ****: $p < 0.0001$).

large number of dead cells appeared in the control group and the AFS group, while the number of dead cells in the SDF-1α/PAFS group was significantly reduced (Fig. 4B). Further quantitative analysis of CCK-8 showed similar results, with the SDF-1α/PAFS group having the highest cell viability (Fig. 4C). Finally, we also used a 2′,7′-dichlorofluorescein diacetate (DCFH-DA) probe to detect the intracellular ROS levels of BMSCs in different groups under oxidative stress. The control group without scaffolds showed the highest intracellular ROS level, while the SDF-1α/PAFS group showed the lowest ROS fluorescence intensity (Fig. 4D). Further quantitative analysis of fluorescence intensity showed similar results, with the fluorescence intensity of the SDF-1α/PAFS group comparable to that of the control group without H_2O_2 (Fig. S2C). From the comprehensive results of the above multiple aspects, we can confirm that SDF-1α/PAFS had good ROS scavenging activity.

3.6. Immunomodulation of scaffolds

Considering the pro-inflammatory microenvironment at the bone defect site and the possible recruitment of inflammatory cells by SDF-1α, the immunomodulatory activity of the scaffolds is crucial. We used RAW264.7 cells to evaluate the immunomodulatory activity of the scaffolds. We first collected the supernatant of the medium after co-culture and measured the concentrations of TNF-α and IL-10. We found that the TNF-α concentration in the SDF-1α/PAFS group was significantly lower than that in the AFS group, but its IL-10 concentration was higher than that in the AFS group (Fig. 5A). Next, we further evaluated the expression of mRNA and marker proteins. The mRNA expression levels of CD86 (Fig. 5B) and TNF-α (Fig. S2D) in the SDF-1α/PAFS group were lower than those in the AFS group, but the mRNA expression of CD206 was higher than that in the AFS group (Fig. 5B). IF

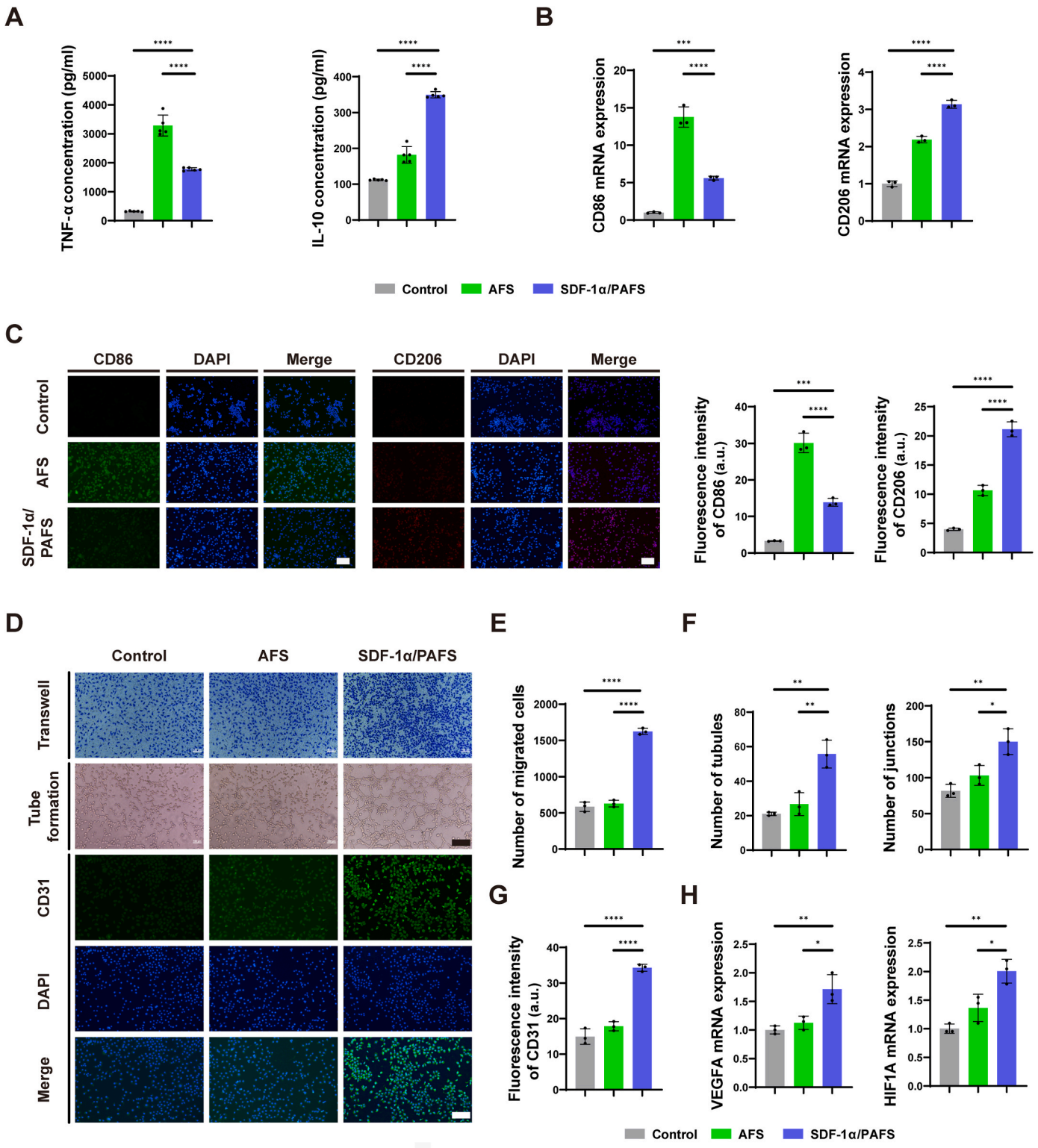

Fig. 5. Immunomodulation and angiogenesis of scaffolds. **A.** The contents of TNF-α and IL-10 of the supernatants of RAW264.7 cells under the stimulation of different scaffolds. The mRNA expression levels (**B**) and IF staining (**C**) of CD86 and CD206 in RAW264.7 cells under the stimulation of different scaffolds. The representative images (**D**) and quantitative analysis (**E, F** and **G**) of Transwell assay, tube formation assay, and IF staining of CD31 under the influence of different scaffolds. **H.** The mRNA expression levels of VEGFA and HIF1A in HUVECs. The results were presented as mean ± SD (ns: no significant differences, *: $p < 0.05$, **: $p < 0.01$, ***: $p < 0.001$, ****: $p < 0.0001$).

staining showed similar results (Fig. 5C), with the highest expression level of M1 marker protein (CD86) in the AFS group while the highest expression level of M2 marker protein (CD206) in the SDF-1α/PAFS group. From the above results, it can be seen that SDF-1α/PAFS tends to induce macrophages to polarize toward M2 and exert anti-inflammatory effects.

3.7. Angiogenesis of scaffolds

To evaluate the angiogenic activity of the scaffolds, we used HUVECs to evaluate it by Transwell and tube formation assays. As shown in Fig. 5D, after 24 h of culture, SDF-1α/PAFS significantly promoted the migration of HUVECs. The number of migrated cells in the AFS group and the control group was similar, and the number of migrated cells in the SDF-1α/PAFS group was significantly more than that in the other groups (Fig. 5E). Moreover, the tube formation assay showed that SDF-1α/PAFS promoted HUVECs to form more tube-like structures (Fig. 5D). The quantitative results also showed that the SDF-1α/PAFS group had the most tubules and junctions (Fig. 5F). IF staining of CD31 and quantitative analysis showed the protein expression level of CD31 in the SDF-1α/PAFS group was the highest among all groups (Fig. 5D and G). The expression of angiogenesis-related genes (VEGFA and HIF1A) was further detected by qRT-PCR. The results showed that the mRNA

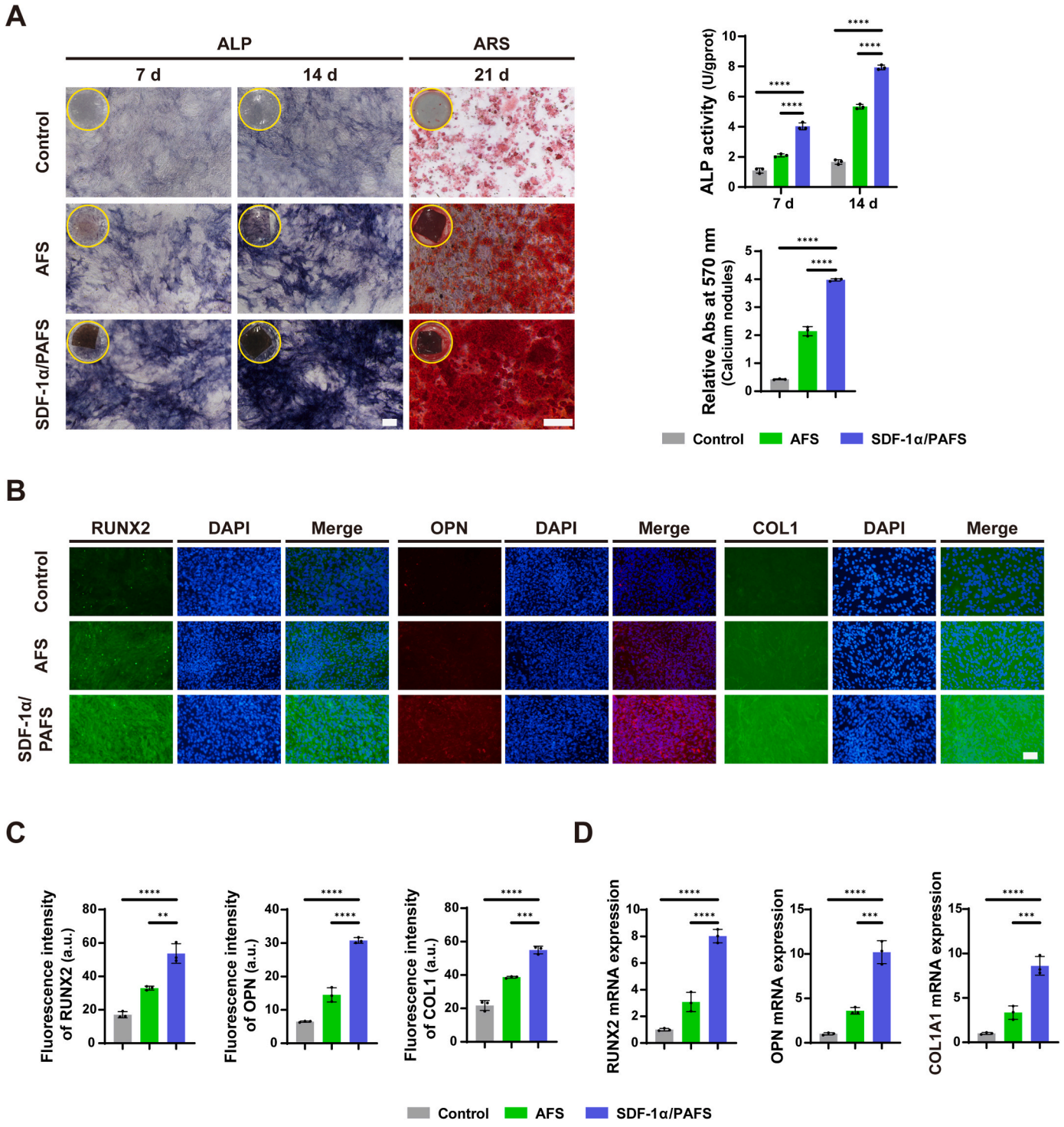

Fig. 6. Osteogenic differentiation in vitro. **A.** The representative images of ALP and ARS staining, and semi-quantitative analysis of ALP activity and calcium nodules. Scale bar = 200 μm. **B-C.** IF staining of RUNX2, OPN, and COL1 in BMSCs. Scale bar = 100 μm. **D.** The mRNA expression levels of RUNX2, OPN, and COL1A1 in BMSCs. The results were presented as mean ± SD (ns: no significant differences, *: $p < 0.05$, **: $p < 0.01$, ***: $p < 0.001$, ****: $p < 0.0001$).

expression levels of VEGFA and HIF1A in the SDF-1α/PAFS group were higher than those in the other groups (Fig. 5H). Therefore, SDF-1α/PAFS can enhance angiogenesis.

3.8. Osteogenic differentiation in vitro

The osteogenic differentiation ability of the scaffolds was the focus of our evaluation. We evaluated the osteogenic ability of the scaffolds from the perspective of ALP activity, calcium nodule deposition, and osteogenic marker expression levels. After 7 and 14 days of osteogenic induction, we evaluated ALP activity as an early osteogenic indicator. As expected, the SDF-1α/PAFS group showed the highest ALP activity, both by ALP staining and quantitative analysis (Fig. 6A). Calcium nodule deposition is an indicator of advanced osteogenesis. After 21 days of culture, calcium nodules appeared in each group by ARS staining, among which the calcium nodules in the SDF-1α/PAFS group were the

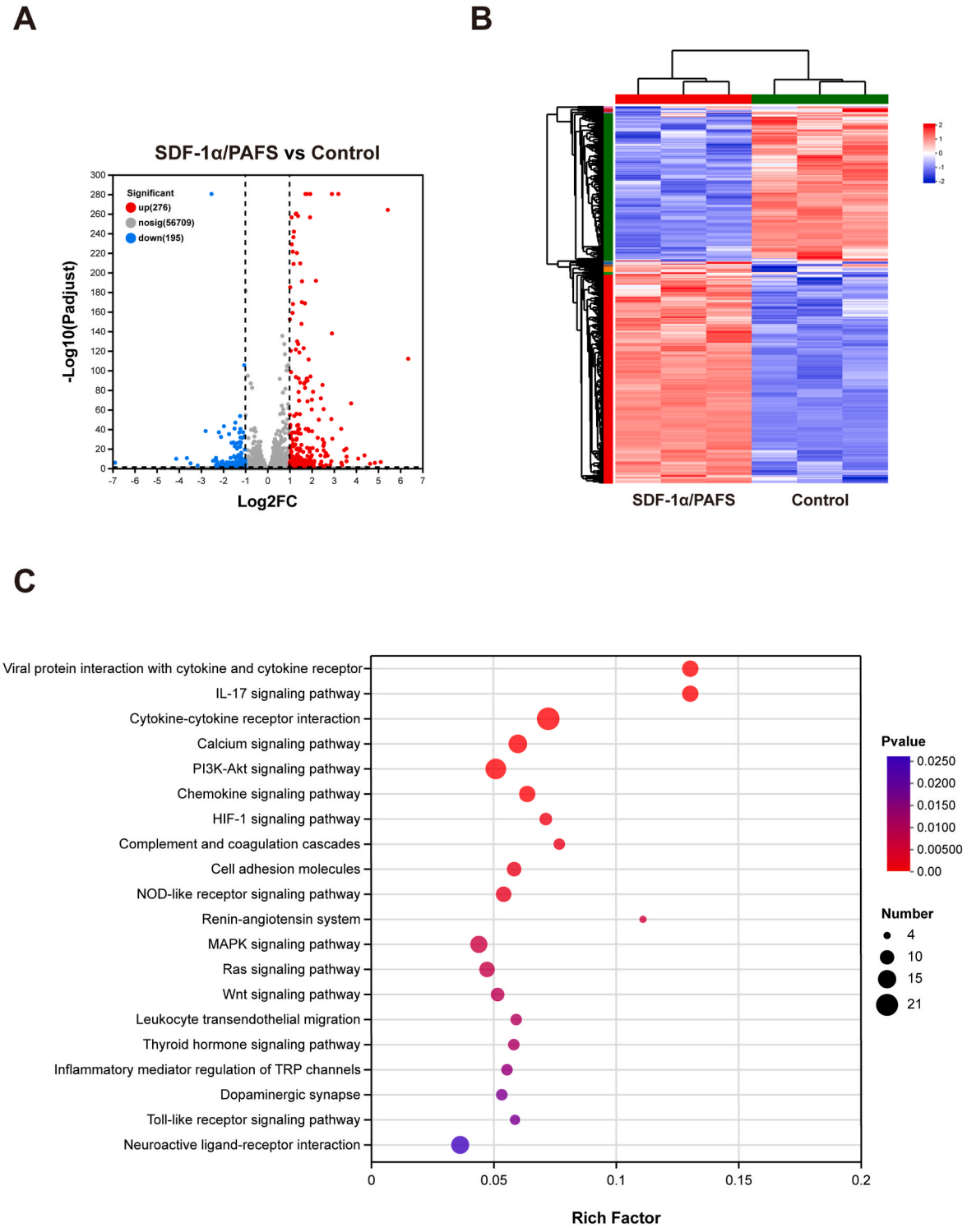

Fig. 7. Transcriptome analysis. The volcano plot (**A**) and Heatmap (**B**) of SDF-1α/PAFS group vs. control group differential genes. **C.** The top 20 enrichment of KEGG pathways (Category: Environmental Information Processing and Cellular Processes) in the SDF-1α/PAFS group compared with the control group.

most obvious, followed by the AFS group (Fig. 6A). Quantitative analysis showed similar results, with the SDF-1α/PAFS group having the largest number of calcium nodules (Fig. 6A). We further determined the expression levels of osteogenic markers (RUNX2, OPN, and COL1) by IF staining and qRT-PCR. The results showed that the protein and mRNA expression levels of these osteogenic markers in the SDF-1α/PAFS group were the highest among all groups (Fig. 6B, C, and D). The excellent osteogenic ability of SDF-1α/PAFS has been confirmed.

Furthermore, we performed RNA transcriptome sequencing to reveal the potential mechanism of osteogenesis in SDF-1α/PAFS. We found that the gene expression in the SDF-1α/PAFS group was significantly different compared with the control group, with 276 genes up-regulated and 195 genes down-regulated (Fig. 7A and B). Next, the Kyoto Encyclopedia of Genes and Genomes (KEGG) pathway enrichment analysis showed that the up-regulated genes were mainly enriched in some specific pathways, such as Calcium signaling pathway, PI3K-Akt signaling pathway, Chemokine signaling pathway, HIF-1 signaling pathway, Cell adhesion molecules, MAPK signaling pathway and Wnt signaling pathway (Fig. 7C). SDF-1α/PAFS may promote osteogenesis through the above pathways.

3.9. In vivo bone regeneration

We established the mouse cranial bone defect model to evaluate the in vivo bone regeneration ability of the scaffolds. The assessment of SDF-1α release of the scaffolds, tracking of injected BMSCs, and functional evaluation including osteogenesis, immunomodulation, and angiogenesis were performed at different time points after surgery (Fig. 8A).

3.9.1. SDF-1α release in vivo

By measuring the concentration of SDF-1α in serum, we evaluated the release effect of SDF-1α/PAFS in vivo (Fig. 8B). There was no significant difference between the SDF-1α/PAFS + BMSCs group and the control group on the first day after surgery. We speculated that the SDF-1α released by SDF-1α/PAFS had not yet fully diffused into the blood on the first day after surgery. On the third day after surgery, the SDF-1α concentration in the SDF-1α/PAFS + BMSCs group was significantly higher than that in the control group and reached the highest value. Until the ninth day after surgery, the concentration of SDF-1α in the SDF-1α/PAFS + BMSCs group was still higher than that in the control group.

3.9.2. Tracking of injected BMSCs in vivo

To evaluate whether SDF-1α/PAFS can contribute to the targeted migration of injected BMSCs, we tracked the migration of injected BMSCs. BMSCs were pre-labeled with DiR before injection, and samples were detected 8 and 12 days after surgery. In addition, we set up the AFS + BMSCs group as a control (Fig. 8C). Image tracking showed that the positive DiR signal of the two groups was similar on the day of cell injection, but at 8 and 12 days after surgery, the positive DiR signal in the SDF-1α/PAFS + BMSCs group was significantly higher than that in the AFS + BMSCs group. Additionally, we further obtained mouse skull samples, and we found that the positive DiR signal in the bone defect site of the SDF-1α/PAFS + BMSCs group was also significantly higher than that in the AFS + BMSCs group. These results indicated that the SDF-1α/PAFS + BMSCs strategy could effectively recruit injected BMSCs to participate in bone regeneration.

3.9.3. Functional evaluation

Mice were sacrificed 4 and 8 weeks after surgery, respectively, and new bone formation was evaluated using micro-CT and histological staining. The results showed that at 4 weeks after surgery, only a very small amount of new bone was formed in the control group, and the amount of new bone in other groups was significantly higher than that in the control group. Among them, the new bone in the SDF-1α/PAFS + BMSCs group was the most obvious, which was more than that in the SDF-1α/PAFS group and the AFS group (Fig. 8D). As time went by, the amount of new bone in all groups increased. By 8 weeks after surgery, the amount of new bone in the SDF-1α/PAFS + BMSCs group was still the largest, more than the other three groups. In terms of quantitative analysis (Fig. 8D), whether at 4 and 8 weeks after surgery, BV/TV, Tb. N, Tb.Th, and Tb. Sp in the SDF-1α/PAFS + BMSCs group all showed the best effect. H&E and Masson's trichrome staining (Fig. 8E) showed that at 4 and 8 weeks after surgery, there was only a small amount of fibrous tissue in the bone defect area in the control group, and no significant new bone was formed, while new bone was observed in other groups. Among all groups, the largest amount of continuous new bone was observed in the SDF-1α/PAFS + BMSCs group. These results showed that the SDF-1α/PAFS + BMSCs strategy demonstrated the most excellent bone regeneration ability in vivo. We also evaluated the in vivo degradation behavior of scaffolds by H&E and Masson's trichrome staining. At 4 weeks after surgery, the scaffolds showed obvious degradation, and the edges of the scaffolds became irregular and tissue grew into them. By 8 weeks after surgery, as the new bone tissue further increased, most of the scaffolds degraded. As a biological scaffold with similar composition to bone tissue, the degradation products of the scaffolds can be directly utilized for bone regeneration. SDF-1α/PAFS has a good match between biodegradation and bone regeneration. In addition, we also obtained H&E staining images of the viscera of mice, and the results showed that the scaffolds had good biological safety (Fig. S4).

Furthermore, we used immunohistochemical staining to evaluate the expression levels of immunomodulation-related proteins (CD86 and CD206), osteogenesis-related proteins (RUNX2 and OCN), and angiogenesis-related proteins (CD31 and EMCN) (Fig. 9). We harvested mouse skulls at 2 weeks after surgery to evaluate the immunomodulatory effect of the scaffolds. The results showed that the expression levels of CD86 and CD206 in the control group were low, while the AFS group showed the highest level of CD86 expression. The expression levels of CD86 in the SDF-1α/PAFS group and the SDF-1α/PAFS + BMSCs group were lower than those in the AFS group. However, the expression levels of CD206 in the SDF-1α/PAFS group and the SDF-1α/PAFS + BMSCs group were significantly higher than those in the AFS group (Fig. S3). SDF-1α/PAFS also tends to induce macrophages to polarize towards M2 in vivo and exert anti-inflammatory effects. Immunohistochemical staining of osteogenesis-related proteins and angiogenesis-related proteins was performed 4 and 8 weeks after surgery. As expected, the expression levels of RUNX2 and OCN in the SDF-1α/PAFS + BMSCs group were the highest among all groups (Fig. S3). Regarding angiogenesis, the expression levels of CD31 and EMCN in the control group and AFS group were low, while the expression levels of CD31 and EMCN proteins in the SDF-1α/PAFS group and the SDF-1α/PAFS + BMSCs group were significantly higher than those in other groups (Fig. S3). It can be seen that SDF-1α/PAFS also shows significant promoting angiogenesis in vivo.

4. Discussion

Bone tissue engineering is gradually replacing traditional methods as a promising method to repair bone defects. Patients with bone defects often suffer from multiple diseases, resulting in low activity of endogenous BMSCs, poor migration ability, and reduced osteogenic differentiation activity [12–15]. This limits the role of endogenous BMSCs in repairing bone defects. At present, bone tissue engineering technology is committed to constructing grafts loaded with normally active BMSCs in vitro and then implanting them into the body to repair bone defects. However, in addition to the troublesome and complicated construction process, this method also faces the challenge of only a few cells playing a repair role after implantation in the body due to various factors [12,16,17]. These problems make it difficult to apply traditional bone tissue-engineered grafts in clinical practice. To this end, we developed a chemotactic cell-free scaffold that can recruit normal BMSCs injected postoperatively to the bone defect site in vivo. This bone defect repair

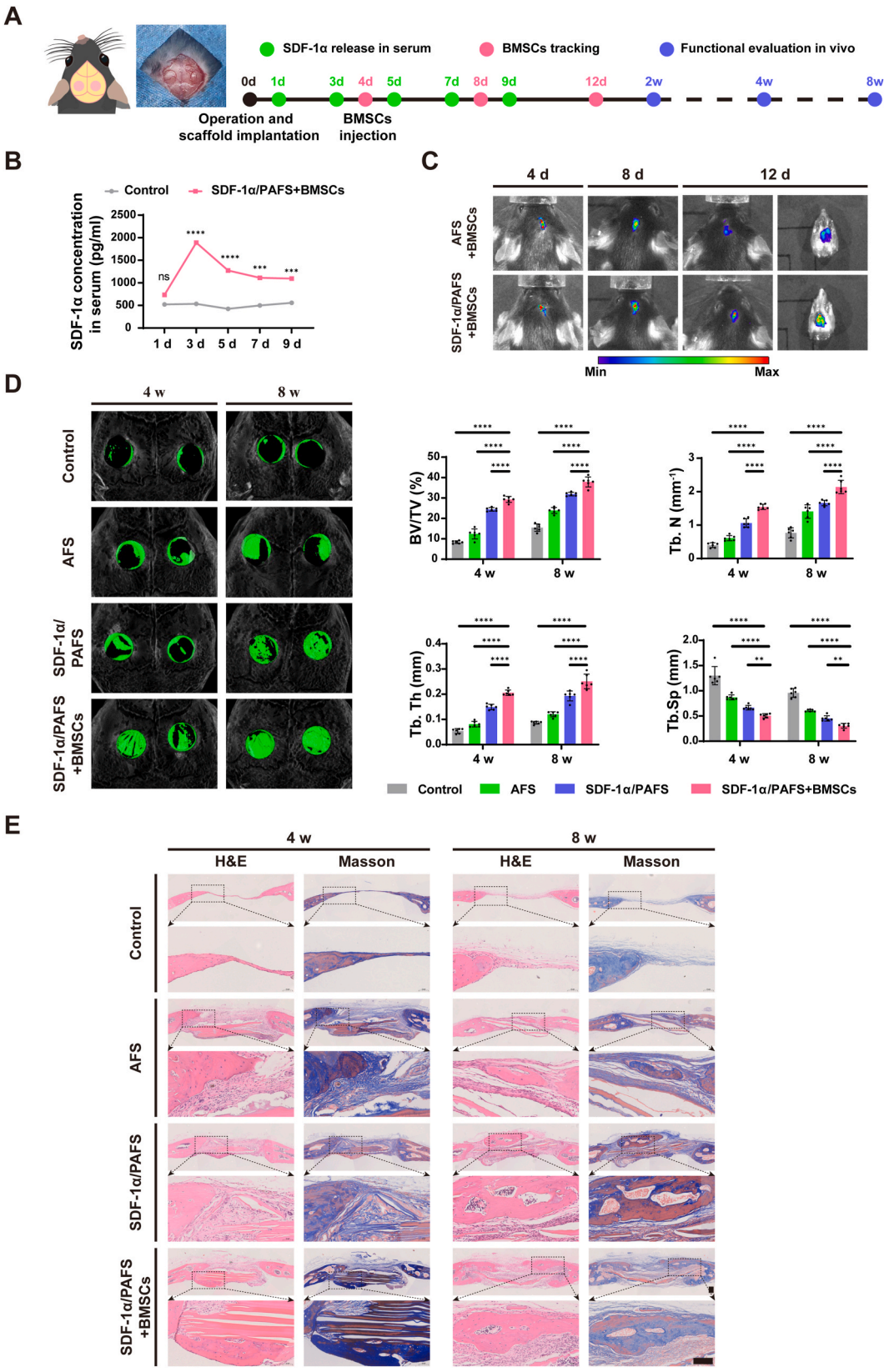

Fig. 8. In vivo bone regeneration. **A.** Experimental procedure of the mice cranial bone defect model. **B.** Concentration of SDF-1α in serum after the implantation of SDF-1α/PAFS. **C.** IVIS imaging system showed the tracking of injected BMSCs in vivo. **D.** Micro-CT reconstruction and quantitative analysis of skull samples in mice at 4 and 8 weeks after surgery. **E.** H&E and Masson trichrome staining of sections of bone defect region. Scale bar = 100 μm. The results were presented as mean ± SD (ns: no significant differences, *: $p < 0.05$, **: $p < 0.01$, ***: $p < 0.001$, ****: $p < 0.0001$).

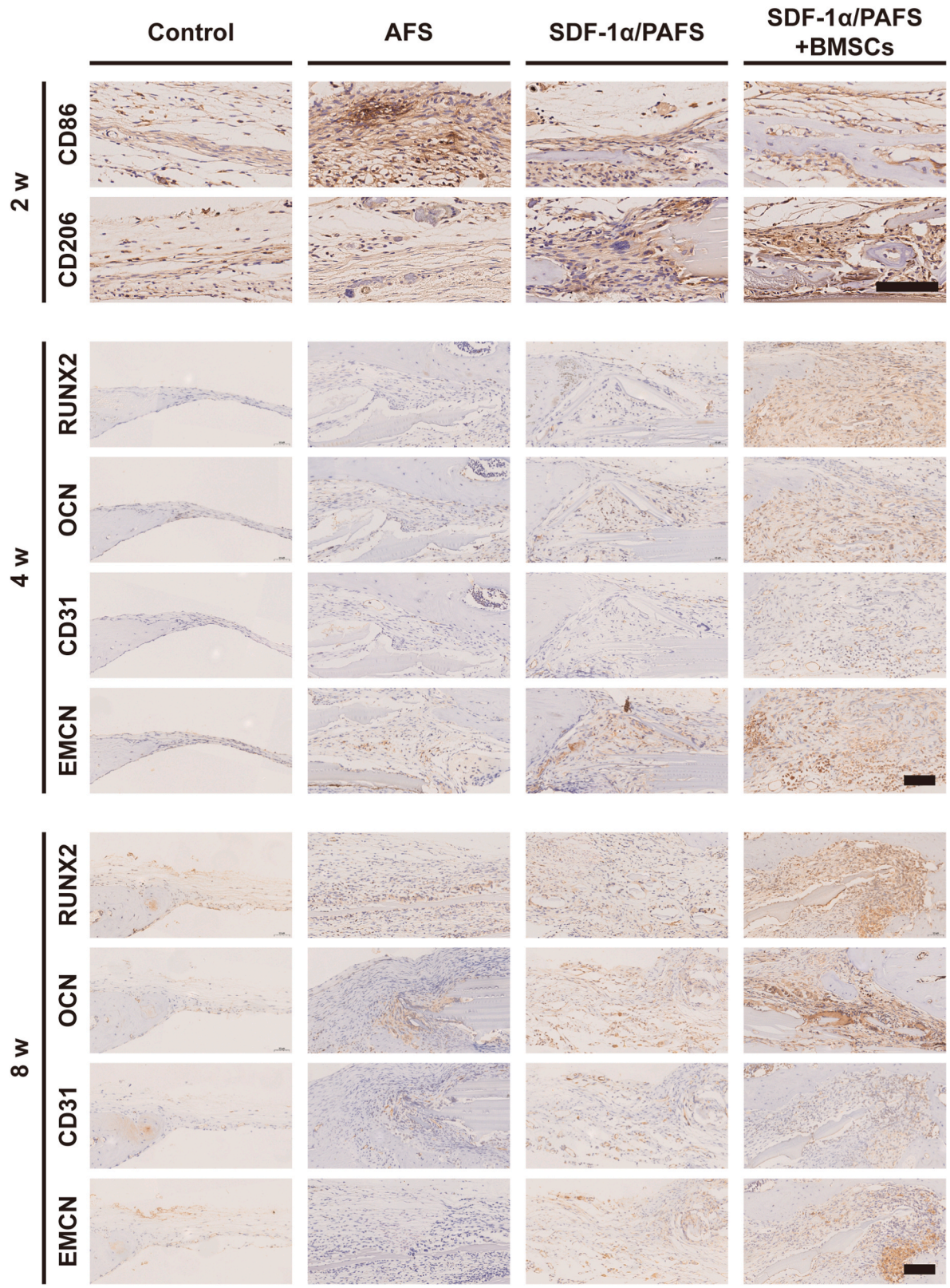

Fig. 9. Immunohistochemical staining of CD86 and CD206 at 2 weeks after surgery, and RUNX2, OCN, CD31, and EMCN at 4 and 8 weeks after surgery. Scale bar = 100 μm.

strategy based on scaffold combined with BMSCs injection can avoid the above problems and promote bone regeneration to complete the repair of bone defects. This bone defect repair strategy has very good clinical convenience.

AFS has attracted attention in bone tissue engineering in recent years [9–11]. Due to its similar composition to bone tissue, mainly composed of collagen and hydroxyapatite [6], AFS has excellent osteogenic ability [9–11]. Moreover, this scaffold based on an acellular matrix also has

good biocompatibility and low immunogenicity [7]. We also found that the surfaces of AFS and SDF-1α/PAFS have characteristic three-dimensional structures. Many studies are currently committed to building similar three-dimensional structures on scaffolds, which trigger specific responses of cells, such as adhesion [48], migration [49], and differentiation [50]. However, most of the preparation methods used in these studies are very complicated, such as electrospinning, directional freezing, and micro-patterning [51]. AFS and SDF-1α/PAFS naturally have characteristic three-dimensional structures and are ideal candidates for three-dimensional tissue engineering. In this study, it was found that the mechanical properties of SDF-1α/PAFS can reach 6.01 ± 1.90 GPa. The Young's modulus of SDF-1α/PAFS is close to that of cortical bone and acellular bone matrix [52], which provides good early mechanical support while also avoiding the occurrence of stress shielding. Such excellent mechanical properties are unmatched by other acellular matrix materials. Multiple studies have also focused on adding complex components to scaffolds based on acellular matrices and hydrogels to improve the mechanical properties of scaffolds [53–55]. SDF-1α/PAFS naturally has excellent mechanical properties. As a biological scaffold with similar composition to bone tissue, SDF-1α/PAFS also showed good matching between biodegradation and bone regeneration. Although the acellular bone matrix has better similarity to natural bone, its limited source and bioethical issues limit its widespread application possibility [52]. Fish scales have long been used as biological waste, with extensive sources and low cost. This is also a major advantage for future applications.

Some studies have developed scaffolds loaded with SDF-1α to recruit endogenous cells [34,56,57]. However, most of the methods to load SDF-1α in these studies are direct protein incorporation and encapsulation inside the scaffold. These scaffolds generally face the problem of initial explosive release, with a short release time, mostly within 7 days [34,56,57]. Moreover, there is also concern about the loss of SDF-1α activity when it is directly encapsulated inside the scaffold. Chen et al. used gene editing to prepare recombinant SDF-1α to develop a scaffold that can slowly release SDF-1α for rotator cuff enthesis regeneration [58]. It provides us with a new idea, but the preparation method is complicated and costly. In addition, these studies have ignored a key issue: SDF-1α not only recruits endogenous stem cells such as BMSCs but also recruits too many inflammatory cells [28,29]. This is unfavorable for bone defects that are already in a state of inflammatory disorder. This may offset endogenous stem cell-mediated tissue repair and even aggravate the damage. PDA can kill three birds with one stone, which not only solves the above two difficulties but also enhances the cell adhesion of the scaffold. Taking advantage of the special viscosity of PDA, SDF-1α/PAFS could release SDF-1α in vivo for at least 10 days, which was the main reason why BMSCs injected after surgery could effectively migrate to bone defects 12 days after surgery. Furthermore, SDF-1α/PAFS could induce M2 polarization of macrophages in vitro and in vivo, playing an anti-inflammatory effect. This immunomodulatory activity not only improved the microenvironment of bone defects but also solved the problem of SDF-1α recruiting too many inflammatory cells. Finally, SDF-1α/PAFS also had better cell adhesion, which played an important role in the colonization and repair of BMSCs.

Regarding the problem of insufficient vitality of endogenous BMSCs, studies have shown that injection of normally active BMSCs can effectively improve bone defect repair [59–61]. In addition, the injection of stem cells has been widely used in the treatment of knee osteoarthritis in clinical practice [62,63]. These provide an important scientific basis for our study. Chen et al. [58] and Hu et al. [33] respectively constructed similar chemotactic cell-free scaffolds combined with stem cell injection for rotator cuff enthesis regeneration and anterior cruciate ligament regeneration, and both showed good results. In our study, the bone regeneration effect of the SDF-1α/PAFS + BMSCs group was significantly better than that of the SDF-1α/PAFS group, which was also due to the targeted repair of BMSCs injected. There were some possible mechanisms by which the SDF-1α/PAFS + BMSCs group enhanced new bone formation: first, SDF-1α/PAFS reduced the level of ROS in bone defects and played an immunomodulatory role to improve the microenvironment; then endogenous BMSCs and BMSCs injected were recruited to bone defects and underwent proliferation and osteogenic differentiation; third, SDF-1α might also mobilize endothelial progenitor cells and create a pro-angiogenic microenvironment, further promoting local angiogenesis and bone regeneration. Some studies usually set the time point for cell injection on the first day after surgery [33,64]. However, in the early postoperative period, especially in the first three days, a large number of inflammatory cells will infiltrate into the defect site, causing a strong inflammatory reaction [65]. Studies have shown that inflammation can lead to stem cell dysfunction [66]. This is also a dilemma faced by grafts loaded with seed cells in vitro. We set the time point for cell injection on the fourth day after surgery, when the edema and peak inflammation at the surgical site have subsided, which can avoid stem cell dysfunction caused by strong inflammation to a certain extent. Our results also showed that the concentration of SDF-1α in serum peaked on the third day after surgery. Overall, the fourth day after surgery is the suitable time point for cell injection in mice. However, there are differences in biological behavior between humans and mice. More studies are needed on the best time point for cell injection in humans. Traditional bone tissue engineering uses complex methods to cultivate grafts in vitro and requires immense care. The grafts also need to face strong inflammation in the early stages of implantation, which limits their clinical application. Our strategy of implanting scaffolds and cells separately effectively avoids the above problems and provides convenience for its future clinical applications. Of course, our strategy is still in the preliminary stage, and experimental verification of large animals and rigorous preclinical trials are needed before entering clinical application.

In summary, we have developed a new strategy for bone defect repair, in which acellular fish scale scaffolds that can continuously release SDF-1α combined with BMSCs injection can effectively promote bone regeneration. This strategy improves the shortcomings of traditional bone tissue engineering grafts and has better clinical convenience and operability. However, our study also has some limitations. First of all, only the scales of grass carp were selected in the study, and the scales of different fish may be different. Second, only one SDF-1α loading concentration and one injected cell number were studied. Further optimizing the SDF-1α loading amount and the injected cell number may be of great significance for bone regeneration. Third, we have only carried out a preliminary exploration of the bone regeneration mechanism of SDF-1α/PAFS, and more experiments are needed to clarify it in depth.

5. Conclusion

In this study, we prepared a polydopamine-functionalized acellular fish scale scaffold capable of sustained release of SDF-1α, which can recruit exogenous BMSCs, and also has ROS scavenging activity, immunomodulation, angiogenesis, and osteogenesis. Based on this, we developed a novel strategy for the treatment of bone defects of combining postoperative injection of BMSCs and SDF-1α/PAFS, which can effectively promote bone regeneration, thereby avoiding the shortcomings of traditional bone tissue grafts. This strategy has better clinical convenience and operability.

CRediT authorship contribution statement

Shilong Su: Writing – review & editing, Writing – original draft, Software, Methodology, Data curation, Conceptualization. **Jinwu Bai:** Writing – review & editing, Software, Methodology, Data curation. **Ruideng Wang:** Writing – review & editing, Software, Data curation. **Shan Gao:** Writing – review & editing, Visualization, Supervision. **Rubing Zhou:** Writing – review & editing, Visualization, Supervision. **Fang Zhou:** Writing – review & editing, Visualization, Validation,

Funding acquisition, Conceptualization.

Funding

This study was supported by the National Natural Science Foundation of China (No. 81971160).

Declaration of competing interest

The authors declare that they have no known competing financial interests or personal relationships that could have appeared to influence the work reported in this paper.

Acknowledgement

The authors would like to thank Shiyanjia Lab (www.shiyanjia.com) for the AFM analysis.

Appendix A. Supplementary data

Supplementary data to this article can be found online at https://doi.org/10.1016/j.mtbio.2025.101759.

Data availability

Data will be made available on request.

References

[1] C. Xie, J. Ye, R. Liang, X. Yao, X. Wu, Y. Koh, et al., Advanced strategies of biomimetic tissue-engineered grafts for bone regeneration, Adv. Healthcare Mater. 10 (14) (2021) e2100408, https://doi.org/10.1002/adhm.202100408.
[2] M. Wu, H. Liu, D. Li, Y. Zhu, P. Wu, Z. Chen, et al., Smart-responsive multifunctional therapeutic system for improved regenerative microenvironment and accelerated bone regeneration via mild photothermal therapy, Adv. Sci. (Weinh.) 11 (2) (2024) e2304641, https://doi.org/10.1002/advs.202304641.
[3] M. Wu, H. Liu, Y. Zhu, F. Chen, Z. Chen, L. Guo, et al., Mild photothermal-stimulation based on injectable and photocurable hydrogels orchestrates immunomodulation and osteogenesis for high-performance bone regeneration, Small 19 (28) (2023) e2300111, https://doi.org/10.1002/smll.202300111.
[4] H. Amirazad, M. Dadashpour, N. Zarghami, Application of decellularized bone matrix as a bioscaffold in bone tissue engineering, J. Biol. Eng. 16 (1) (2022) 1, https://doi.org/10.1186/s13036-021-00282-5.
[5] C.W. Cheng, L.D. Solorio, E. Alsberg, Decellularized tissue and cell-derived extracellular matrices as scaffolds for orthopaedic tissue engineering, Biotechnol. Adv. 32 (2) (2014) 462–484, https://doi.org/10.1016/j.biotechadv.2013.12.012.
[6] H. Feng, X. Li, X. Deng, X. Li, J. Guo, K. Ma, et al., The lamellar structure and biomimetic properties of a fish scale matrix, RSC Adv. 10 (2) (2020) 875–885, https://doi.org/10.1039/c9ra08189e.
[7] L. Salvatore, N. Gallo, M.L. Natali, L. Campa, P. Lunetti, M. Madaghiele, et al., Marine collagen and its derivatives: versatile and sustainable bio-resources for healthcare, Mater. Sci. Eng., C 113 (2020) 110963, https://doi.org/10.1016/j.msec.2020.110963.
[8] E.A. Zimmermann, B. Gludovatz, E. Schaible, N.K. Dave, W. Yang, M.A. Meyers, et al., Mechanical adaptability of the Bouligand-type structure in natural dermal armour, Nat. Commun. 4 (2013) 2634, https://doi.org/10.1038/ncomms3634.
[9] Y. Wang, B. Kong, X. Chen, R. Liu, Y. Zhao, Z. Gu, et al., BMSC exosome-enriched acellular fish scale scaffolds promote bone regeneration, J. Nanobiotechnol. 20 (1) (2022) 444, https://doi.org/10.1186/s12951-022-01646-9.
[10] W. Wu, Z. Zhou, G. Sun, Y. Liu, A. Zhang, X. Chen, Construction and characterization of degradable fish scales for enhancing cellular adhesion and potential using as tissue engineering scaffolds, Mater. Sci. Eng., C 122 (2021) 111919, https://doi.org/10.1016/j.msec.2021.111919.
[11] A. Kara, S. Tamburaci, F. Tihminlioglu, H. Havitcioglu, Bioactive fish scale incorporated chitosan biocomposite scaffolds for bone tissue engineering, Int. J. Biol. Macromol. 130 (2019) 266–279, https://doi.org/10.1016/j.ijbiomac.2019.02.067.
[12] B.D. Sui, C.H. Hu, A.Q. Liu, C.X. Zheng, K. Xuan, Y. Jin, Stem cell-based bone regeneration in diseased microenvironments: challenges and solutions, Biomaterials 196 (2019) 18–30, https://doi.org/10.1016/j.biomaterials.2017.10.046.
[13] K.I. Ko, L.S. Coimbra, C. Tian, J. Alblowi, R.A. Kayal, T.A. Einhorn, et al., Diabetes reduces mesenchymal stem cells in fracture healing through a TNFalpha-mediated mechanism, Diabetologia 58 (3) (2015) 633–642, https://doi.org/10.1007/s00125-014-3470-y.
[14] B.D. Sui, C.H. Hu, C.X. Zheng, Y. Jin, Microenvironmental views on mesenchymal stem cell differentiation in aging, J. Dent. Res. 95 (12) (2016) 1333–1340, https://doi.org/10.1177/0022034516653589.
[15] B. Sui, C. Hu, L. Liao, Y. Chen, X. Zhang, X. Fu, et al., Mesenchymal progenitors in osteopenias of diverse pathologies: differential characteristics in the common shift from osteoblastogenesis to adipogenesis, Sci. Rep. 6 (2016) 30186, https://doi.org/10.1038/srep30186.
[16] A. Ho-Shui-Ling, J. Bolander, L.E. Rustom, A.W. Johnson, F.P. Luyten, C. Picart, Bone regeneration strategies: engineered scaffolds, bioactive molecules and stem cells current stage and future perspectives, Biomaterials 180 (2018) 143–162, https://doi.org/10.1016/j.biomaterials.2018.07.017.
[17] A. Kurtz, Mesenchymal stem cell delivery routes and fate, Int J Stem Cells 1 (1) (2008) 1–7, https://doi.org/10.15283/ijsc.2008.1.1.1.
[18] A.T. Askari, S. Unzek, Z.B. Popovic, C.K. Goldman, F. Forudi, M. Kiedrowski, et al., Effect of stromal-cell-derived factor 1 on stem-cell homing and tissue regeneration in ischaemic cardiomyopathy, Lancet 362 (9385) (2003) 697–703, https://doi.org/10.1016/S0140-6736(03)14232-8.
[19] S.W. Lewellis, H. Knaut, Attractive guidance: how the chemokine SDF1/CXCL12 guides different cells to different locations, Semin. Cell Dev. Biol. 23 (3) (2012) 333–340, https://doi.org/10.1016/j.semcdb.2012.03.009.
[20] A. Dar, P. Goichberg, V. Shinder, A. Kalinkovich, O. Kollet, N. Netzer, et al., Chemokine receptor CXCR4-dependent internalization and resecretion of functional chemokine SDF-1 by bone marrow endothelial and stromal cells, Nat. Immunol. 6 (10) (2005) 1038–1046, https://doi.org/10.1038/ni1251.
[21] J. Deshane, S. Chen, S. Caballero, A. Grochot-Przeczek, H. Was, Calzi S. Li, et al., Stromal cell-derived factor 1 promotes angiogenesis via a heme oxygenase 1-dependent mechanism, J. Exp. Med. 204 (3) (2007) 605–618, https://doi.org/10.1084/jem.20061609.
[22] S. Otsuru, K. Tamai, T. Yamazaki, H. Yoshikawa, Y. Kaneda, Circulating bone marrow-derived osteoblast progenitor cells are recruited to the bone-forming site by the CXCR4/stromal cell-derived factor-1 pathway, Stem Cell. 26 (1) (2008) 223–234, https://doi.org/10.1634/stemcells.2007-0515.
[23] H. Shichinohe, S. Kuroda, S. Yano, K. Hida, Y. Iwasaki, Role of SDF-1/CXCR4 system in survival and migration of bone marrow stromal cells after transplantation into mice cerebral infarct, Brain Res. 1183 (2007) 138–147, https://doi.org/10.1016/j.brainres.2007.08.091.
[24] A. Cipitria, K. Boettcher, S. Schoenhals, D.S. Garske, K. Schmidt-Bleek, A. Ellinghaus, et al., In-situ tissue regeneration through SDF-1alpha driven cell recruitment and stiffness-mediated bone regeneration in a critical-sized segmental femoral defect, Acta Biomater. 60 (2017) 50–63, https://doi.org/10.1016/j.actbio.2017.07.032.
[25] R.M. Raftery, A.G. Gonzalez Vazquez, D.P. Walsh, G. Chen, A.L. Laiva, M.B. Keogh, et al., Mobilizing endogenous progenitor cells using pSDF1alpha-activated scaffolds accelerates angiogenesis and bone repair in critical-sized bone defects, Adv. Healthcare Mater. 13 (23) (2024) e2401031, https://doi.org/10.1002/adhm.202401031.
[26] Q. Chen, C. Zheng, Y. Li, S. Bian, H. Pan, X. Zhao, et al., Bone targeted delivery of SDF-1 via alendronate functionalized nanoparticles in guiding stem cell migration, ACS Appl. Mater. Interfaces 10 (28) (2018) 23700–23710, https://doi.org/10.1021/acsami.8b08606.
[27] D.K. Jin, K. Shido, H.G. Kopp, I. Petit, S.V. Shmelkov, L.M. Young, et al., Cytokine-mediated deployment of SDF-1 induces revascularization through recruitment of CXCR4+ hemangiocytes, Nat Med 12 (5) (2006) 557–567, https://doi.org/10.1038/nm1400.
[28] M.C. Ghosh, G.D. Collins, B. Vandanmagsar, K. Patel, M. Brill, A. Carter, et al., Activation of Wnt5A signaling is required for CXC chemokine ligand 12-mediated T-cell migration, Blood 114 (7) (2009) 1366–1373, https://doi.org/10.1182/blood-2008-08-175869.
[29] L. Luo, Y. Li, Z. Bao, D. Zhu, G. Chen, W. Li, et al., Pericardial delivery of SDF-1alpha puerarin hydrogel promotes heart repair and electrical coupling, Adv Mater 36 (1) (2024) e2302686, https://doi.org/10.1002/adma.202302686.
[30] G. Cerqueni, A. Scalzone, C. Licini, P. Gentile, M. Mattioli-Belmonte, Insights into oxidative stress in bone tissue and novel challenges for biomaterials, Mater. Sci. Eng., C 130 (2021) 112433, https://doi.org/10.1016/j.msec.2021.112433.
[31] P. Qiu, M. Li, K. Chen, B. Fang, P. Chen, Z. Tang, et al., Periosteal matrix-derived hydrogel promotes bone repair through an early immune regulation coupled with enhanced angio- and osteogenesis, Biomaterials 227 (2020) 119552, https://doi.org/10.1016/j.biomaterials.2019.119552.
[32] Y. Zhu, H. Liu, P. Wu, Y. Chen, Z. Deng, L. Cai, et al., Multifunctional injectable hydrogel system as a mild photothermal-assisted therapeutic platform for programmed regulation of inflammation and osteo-microenvironment for enhanced healing of diabetic bone defects in situ, Theranostics 14 (18) (2024) 7140–7198, https://doi.org/10.7150/thno.102779.
[33] Y. Hu, J. Ran, Z. Zheng, Z. Jin, X. Chen, Z. Yin, et al., Exogenous stromal derived factor-1 releasing silk scaffold combined with intra-articular injection of progenitor cells promotes bone-ligament-bone regeneration, Acta Biomater. 71 (2018) 168–183, https://doi.org/10.1016/j.actbio.2018.02.019.
[34] X. Shen, Y. Zhang, Y. Gu, Y. Xu, Y. Liu, B. Li, et al., Sequential and sustained release of SDF-1 and BMP-2 from silk fibroin-nanohydroxyapatite scaffold for the enhancement of bone regeneration, Biomaterials 106 (2016) 205–216, https://doi.org/10.1016/j.biomaterials.2016.08.023.
[35] H. Lee, S.M. Dellatore, W.M. Miller, P.B. Messersmith, Mussel-inspired surface chemistry for multifunctional coatings, Science 318 (5849) (2007) 426–430, https://doi.org/10.1126/science.1147241.
[36] J. Li, F. Cao, B. Wu, J. Yang, W. Xu, W. Wang, et al., Immobilization of bioactive vascular endothelial growth factor onto Ca-deficient hydroxyapatite-coated Mg by

covalent bonding using polydopamine, J Orthop Translat 30 (2021) 82–92, https://doi.org/10.1016/j.jot.2021.06.002.
[37] X. Zhang, J. Li, J. Chen, Z.X. Peng, J.N. Chen, X. Liu, et al., Enhanced bone regeneration via PHA scaffolds coated with polydopamine-captured BMP2, J. Mater. Chem. B 10 (32) (2022) 6214–6227, https://doi.org/10.1039/d2tb01122k.
[38] X. Bao, J. Zhao, J. Sun, M. Hu, X. Yang, Polydopamine nanoparticles as efficient scavengers for reactive oxygen species in periodontal disease, ACS Nano 12 (9) (2018) 8882–8892, https://doi.org/10.1021/acsnano.8b04022.
[39] J. Li, H. Qiu, H. Gong, W. Tong, Broad-spectrum reactive oxygen species scavenging and activated macrophage-targeting microparticles ameliorate inflammatory bowel disease, Biomacromolecules 22 (7) (2021) 3107–3118, https://doi.org/10.1021/acs.biomac.1c00551.
[40] W. Ma, X. Zhang, Y. Liu, L. Fan, J. Gan, W. Liu, et al., Polydopamine decorated microneedles with Fe-MSC-Derived nanovesicles encapsulation for wound healing, Adv. Sci. (Weinh.) 9 (13) (2022) e2103317, https://doi.org/10.1002/advs.202103317.
[41] Y. Li, L. Yang, Y. Hou, Z. Zhang, M. Chen, M. Wang, et al., Polydopamine-mediated graphene oxide and nanohydroxyapatite-incorporated conductive scaffold with an immunomodulatory ability accelerates periodontal bone regeneration in diabetes, Bioact. Mater. 18 (2022) 213–227, https://doi.org/10.1016/j.bioactmat.2022.03.021.
[42] S. Su, R. Wang, J. Bai, Z. Chen, F. Zhou, Novel decellularization scheme for preparing acellular fish scale scaffolds for bone tissue engineering, ACS Omega 10 (1) (2025) 230–238, https://doi.org/10.1021/acsomega.4c05096.
[43] Y. Tang, C. Chen, F. Liu, S. Xie, J. Qu, M. Li, et al., Structure and ingredient-based biomimetic scaffolds combining with autologous bone marrow-derived mesenchymal stem cell sheets for bone-tendon healing, Biomaterials 241 (2020) 119837, https://doi.org/10.1016/j.biomaterials.2020.119837.
[44] A. Boskey, N. Pleshko Camacho, FT-IR imaging of native and tissue-engineered bone and cartilage, Biomaterials 28 (15) (2007) 2465–2478, https://doi.org/10.1016/j.biomaterials.2006.11.043.
[45] N.T. Khanarian, M.K. Boushell, J.P. Spalazzi, N. Pleshko, A.L. Boskey, H.H. Lu, FTIR-I compositional mapping of the cartilage-to-bone interface as a function of tissue region and age, J. Bone Miner. Res. 29 (12) (2014) 2643–2652, https://doi.org/10.1002/jbmr.2284.
[46] Y. Zhou, C. Chen, Z. Guo, S. Xie, J. Hu, H. Lu, SR-FTIR as a tool for quantitative mapping of the content and distribution of extracellular matrix in decellularized book-shape bioscaffolds, BMC Musculoskelet Disord 19 (1) (2018) 220, https://doi.org/10.1186/s12891-018-2149-9.
[47] P.M. Crapo, T.W. Gilbert, S.F. Badylak, An overview of tissue and whole organ decellularization processes, Biomaterials 32 (12) (2011) 3233–3243, https://doi.org/10.1016/j.biomaterials.2011.01.057.
[48] D. Khang, J. Lu, C. Yao, K.M. Haberstroh, T.J. Webster, The role of nanometer and sub-micron surface features on vascular and bone cell adhesion on titanium, Biomaterials 29 (8) (2008) 970–983, https://doi.org/10.1016/j.biomaterials.2007.11.009.
[49] H. Jeon, S. Koo, W.M. Reese, P. Loskill, C.P. Grigoropoulos, K.E. Healy, Directing cell migration and organization via nanocrater-patterned cell-repellent interfaces, Nat. Mater. 14 (9) (2015) 918–923, https://doi.org/10.1038/nmat4342.
[50] M. Zhu, H. Ye, J. Fang, C. Zhong, J. Yao, J. Park, et al., Engineering high-resolution micropatterns directly onto titanium with optimized contact guidance to promote osteogenic differentiation and bone regeneration, ACS Appl. Mater. Interfaces 11 (47) (2019) 43888–43901, https://doi.org/10.1021/acsami.9b16050.
[51] X. Lin, B. Kong, Y. Zhu, Y. Zhao, Bioactive fish scale scaffolds with MSCs-loading for skin flap regeneration, Adv. Sci. (Weinh.) 9 (21) (2022) e2201226, https://doi.org/10.1002/advs.202201226.
[52] B.B. Rothrauff, R.S. Tuan, Decellularized bone extracellular matrix in skeletal tissue engineering, Biochem. Soc. Trans. 48 (3) (2020) 755–764, https://doi.org/10.1042/BST20190079.
[53] Z.Y. Chen, S. Gao, R.B. Zhou, R.D. Wang, F. Zhou, Dual-crosslinked networks of superior stretchability and toughness polyacrylamide-carboxymethylcellulose hydrogel for delivery of alendronate, Mater Design 217 (2022), https://doi.org/10.1016/j.matdes.2022.110627.
[54] Y. Yuan, Y. Xu, Y. Mao, H. Liu, M. Ou, Z. Lin, et al., Three birds, one stone: an osteo-microenvironment stage-regulative scaffold for bone defect repair through modulating early osteo-immunomodulation, middle neovascularization, and later osteogenesis, Adv. Sci. (Weinh.) 11 (6) (2024) e2306428, https://doi.org/10.1002/advs.202306428.
[55] M. Wu, H. Liu, Y. Zhu, P. Wu, Y. Chen, Z. Deng, et al., Bioinspired soft-hard combined system with mild photothermal therapeutic activity promotes diabetic bone defect healing via synergetic effects of immune activation and angiogenesis, Theranostics 14 (10) (2024) 4014–4057, https://doi.org/10.7150/thno.97335.
[56] B. Zhang, H. Li, L. He, Z. Han, T. Zhou, W. Zhi, et al., Surface-decorated hydroxyapatite scaffold with on-demand delivery of dexamethasone and stromal cell derived factor-1 for enhanced osteogenesis, Mater. Sci. Eng., C 89 (2018) 355–370, https://doi.org/10.1016/j.msec.2018.04.008.
[57] Y. Mao, Y. Chen, W. Li, Y. Wang, J. Qiu, Y. Fu, et al., Physiology-Inspired multilayer nanofibrous membranes modulating endogenous stem cell recruitment and osteo-differentiation for staged bone regeneration, Adv. Healthcare Mater. 11 (21) (2022) e2201457, https://doi.org/10.1002/adhm.202201457.
[58] C. Chen, Y. Chen, M. Li, H. Xiao, Q. Shi, T. Zhang, et al., Functional decellularized fibrocartilaginous matrix graft for rotator cuff enthesis regeneration: a novel technique to avoid in-vitro loading of cells, Biomaterials 250 (2020) 119996, https://doi.org/10.1016/j.biomaterials.2020.119996.
[59] M.H. Mankani, S.A. Kuznetsov, G.W. Marshall, P.G. Robey, Creation of new bone by the percutaneous injection of human bone marrow stromal cell and HA/TCP suspensions, Tissue Eng Part A 14 (12) (2008) 1949–1958, https://doi.org/10.1089/ten.tea.2007.0348.
[60] G.P. Freitas, H.B. Lopes, P.S. At, F.P.O. Pg, G.A. Al, P.G. Coelho, et al., Effect of cell therapy with osteoblasts differentiated from bone marrow or adipose tissue stromal cells on bone repair, Regen. Med. 14 (12) (2019) 1107–1119, https://doi.org/10.2217/rme-2019-0036.
[61] A.T.P. Souza, G.P. Freitas, H.B. Lopes, D. Weffort, L.F. Adolpho, M.P.O. Gomes, et al., Mesenchymal stem cell-based therapy for osteoporotic bones: effects of the interaction between cells from healthy and osteoporotic rats on osteoblast differentiation and bone repair, Life Sci. 340 (2024) 122463, https://doi.org/10.1016/j.lfs.2024.122463.
[62] J.H. Kim, K.I. Kim, W.K. Yoon, S.J. Song, W. Jin, Intra-articular injection of mesenchymal stem cells after high tibial osteotomy in osteoarthritic knee: two-year follow-up of randomized control trial, Stem Cells Transl Med 11 (6) (2022) 572–585, https://doi.org/10.1093/stcltm/szac023.
[63] S.H. Kim, C.W. Ha, Y.B. Park, E. Nam, J.E. Lee, H.J. Lee, Intra-articular injection of mesenchymal stem cells for clinical outcomes and cartilage repair in osteoarthritis of the knee: a meta-analysis of randomized controlled trials, Arch Orthop Trauma Surg 139 (7) (2019) 971–980, https://doi.org/10.1007/s00402-019-03140-8.
[64] M. Horie, H. Choi, R.H. Lee, R.L. Reger, J. Ylostalo, T. Muneta, et al., Intra-articular injection of human mesenchymal stem cells (MSCs) promote rat meniscal regeneration by being activated to express Indian hedgehog that enhances expression of type II collagen, Osteoarthr. Cartil. 20 (10) (2012) 1197–1207, https://doi.org/10.1016/j.joca.2012.06.002.
[65] C. Schlundt, T. El Khassawna, A. Serra, A. Dienelt, S. Wendler, H. Schell, et al., Macrophages in bone fracture healing: their essential role in endochondral ossification, Bone 106 (2018) 78–89, https://doi.org/10.1016/j.bone.2015.10.019.
[66] C.K. Glass, K. Saijo, B. Winner, M.C. Marchetto, F.H. Gage, Mechanisms underlying inflammation in neurodegeneration, Cell 140 (6) (2010) 918–934, https://doi.org/10.1016/j.cell.2010.02.016.